Stochastic Ion Heating by a Lower Hybrid Wave: II

Charles F. F. Karney

Plasma Physics Laboratory, Princeton University,
Princeton, New Jersey 08544

The motion of an ion in a coherent lower hybrid wave (characterized by $|k_\parallel| \ll |k_\perp|$ and $\omega \gg \Omega_i$) in a tokamak plasma is studied. For ions satisfying $v_\perp > \omega/k_\perp$, the Lorentz force law for the ions is reduced to a set of difference equations which give the Larmor radius and phase of an ion on one cyclotron orbit in terms of these quantities a cyclotron period earlier. From these difference equations an earlier result [Phys. Fluids **21**, 1584 (1978)] that above a certain wave amplitude the ion motion is stochastic, is readily obtained. The stochasticity threshold is given a simple physical interpretation. In addition, the difference equations are used to derive a diffusion equation governing the heating of the ions above the stochasticity threshold. By including the effects of collisions, the heating rate for the bulk ions is obtained.

I. INTRODUCTION

The motion of an ion in a plasma in the presence of a lower hybrid wave becomes stochastic if the amplitude of the lower hybrid wave exceeds a threshold. This provides a mechanism by which ions may be directly heated by the wave when using lower hybrid waves to heat a tokamak plasma. In this paper we extend the work of an earlier paper[1] (henceforth referred to as I), in which the stochasticity threshold was derived. The main objects are to give a simple physical explanation of the stochasticity threshold, to derive the velocity space diffusion coefficient, and hence to determine the heating rate.

In I it was shown that for the purposes of computing the ion motion it may be assumed that the magnetic field is uniform if the fractional change in the magnetic field over a Larmor radius is small. Similarly, the lower hybrid wave may be treated as perpendicularly propagating if the wavevector, $\mathbf{k}$, satisfies $\left|k_\parallel/k_\perp\right| < \frac{1}{2}(\omega/\Omega_i)^{-1/6}$. Both these conditions are well satisfied in normal circumstances. Shear in the magnetic field may also affect the motion;[2] however, if the scale length of the shear greatly exceeds the Larmor radius, we expect that this effect may also be ignored. Thus, in this paper, we consider only the case of an electrostatic wave propagating perpendicularly to a uniform magnetic field; i.e.,

$$\mathbf{B} = B_0\hat{\mathbf{z}}, \qquad \mathbf{E} = E_0\hat{\mathbf{y}}\cos(k_\perp y - \omega t). \tag{1}$$

As in I these fields are taken to be imposed, since only the motion of a small fraction of the ions on the tail of the ion distribution function becomes stochastic, while the bulk ions and electrons support the wave. Having determined the heating rate it will be possible to allow for the damping of the wave.

Following I the Lorentz force law for an ion with mass, m_i, and charge, $q_i = Z_i e$, may be written as

$$\ddot{y} + y = \alpha\cos(y - \nu t), \qquad \dot{x} = y, \tag{2}$$

where length is normalized to $k_\perp^{-1}$ and time to Ω_i^{-1} ($\Omega_i = q_i B_0/m_i$) and where

$$\nu \equiv \omega/\Omega_i, \tag{3a}$$

$$\alpha \equiv \frac{E_0/B_0}{\Omega_i/k_\perp}. \tag{3b}$$

For later use we shall also define a normalized Larmor radius, r, by

$$r \equiv k_\perp v_\perp/\Omega_i, \tag{3c}$$

where $v_\perp^2 = \dot{x}^2 + \dot{y}^2$.

The plan of this paper is as follows: We first reduce the Lorentz force law for the ion, (2), to a set of difference equations (Sec. II) which determine the velocity and phase of the ion in terms of its velocity and phase a cyclotron period earlier. These difference equations have several symmetries which are presented in Sec. III and which simplify the study of the ion motion. This is followed by a study of the ion motion for infinitesimal E_0 (Sec. IV) where we show that the motion when ω is at a harmonic or half harmonic of the cyclotron frequency has a very different character from the motion at other frequencies. In Sec. V we describe qualitatively the motion when E_0 is finite. Here we define the stochasticity threshold and explain it physically. The statisical properties of the ion motion above the stochasticity threshold are described by the Krylov–Kolmogorov–Sinai entropy and the correlation function which are examined in Secs. VI and VII. From the correlation function we

find the diffusion coefficient (Sec. VIII). For times much longer than the correlation time the ion motion in perpendicular velocity space is governed by a diffusion equation which is derived in Sec. IX. This equation is checked against the exact equations of motion by comparing a Monte Carlo solution of the diffusion equation with a simulation described in I. Since the stochastic heating only affects the tail ions we include a collision term in the diffusion equation as a means of heating the bulk ions and electrons. The resulting Fokker–Planck equation which describes the ion motion in two-dimensional velocity space ($v_\perp$ and $v_\parallel$) is reduced to a one-dimensional equation in $v_\perp$ only (Sec. X). The one-dimensional Fokker–Planck equation is checked against the two-dimensional equation by numerically solving each of them (Sec. XI). Analytic steady-state solutions to the one-dimensional equation are derived in Sec. XII which give results for the heating rates of the ions and electrons.

II.   DERIVATION OF THE DIFFERENCE EQUATIONS

In this section we derive difference equations which approximately describe the motion of the ion. The procedure involves integrating the equations of motion along unperturbed orbits. Nonlinearity is introduced because we repeatedly correct the unperturbed trajectories. We assume that the wave frequency is much larger than the cyclotron frequency; i.e., $\omega \gg \Omega_i$ or $\nu \gg 1$. (This is the case for lower hybrid waves.) On a time scale between the wave period and the cyclotron period the ion does not experience the effects of the magnetic field and behaves, in some respects, as though in zero magnetic field. Thus, when it passes through the wave-particle resonance points, $\omega = \mathbf{k}\dot{\mathbf{v}}$ or $\dot{y} = \nu$ (Fig. 1), it will experience kicks, which we can approximate by impulses. This is the physical picture that will guide our derivation. We shall not be too concerned yet about the limits in which our approximations are valid, preferring to rely on physical intuition. Appendix A gives an alternate derivation starting from the Hamiltonian. While this derivation is less transparent, it does enable us to state the limits of validity of the difference equations.

From Fig. 1 we see that for $r > \nu$ the particle passes through wave-particle resonance twice per cyclotron orbit. We will approximate the force on the particle due to the electric field by impulses or delta functions at these two points and zero elsewhere.

In order to evaluate the area of the delta function forces we Taylor-expand the orbit about the wave-particle resonance point using the unperturbed equation of motion, $\ddot{y}+y = 0$. Thus, we have

$$y - \nu t = y_c + \dot{y}(t_c)t' + \tfrac{1}{2}\ddot{y}(t_c)t'^2 - \nu t$$

$$= \phi_c - \tfrac{1}{2}y_c t'^2, \tag{4}$$

where $t' = t - t_c$, $\phi_c = y_c - \nu t_c$, t_c and y_c are the time and position of the wave-particle "collision," and, by assumption, $\dot{y}(t_c) = \nu$. We substitute (4) into the electrostatic force term in (2), $\alpha \cos(y - \nu t)$, and approximate the resulting expression by $B\,\delta(t - t_c)$, where δ is the Dirac delta function and

$$B = \int_{-\infty}^{\infty} \alpha \cos(\phi_c - \tfrac{1}{2}y_c t'^2)dt'$$

$$= \alpha(2\pi/\,|y_c|)^{1/2} \cos[\phi_c - \text{sign}(y_c)\pi/4] \tag{5}$$

[see Ref. 3, Eq. (4.3.144)]. We note that ϕ_c and hence B are the same (to first order in α) whether we compute t_c and y_c from the intersection of the orbit for $t < t_c$ with $\dot{y} = \nu$ or from the intersection of the orbit for $t > t_c$ with $\dot{y} = \nu$. This is so because y_c and t_c are unchanged by the kick the ion receives, and because $d(y - \nu t)/dt = 0$ near the collision (since $\dot{y} = \nu$). As a consequence the mapping we define with the difference equations will be invariant to time reversal, which in turn means that the mapping is measure-preserving, a necessary condition for a non-dissipitive (i.e., Hamiltonian) system.

We define the cyclotron orbit as beginning and ending at $y = 0$, $\dot{y} < 0$ (Fig. 1). Subscript, j, will refer to the orbit at the beginning of the jth or ending of the $(j-1)$th orbit. A subscript, $j + \frac{1}{2}$, will be used to refer to the middle of the jth orbit, where $y = 0$, $\dot{y} > 0$. Finally, subscripts, $+$ and $-$, will refer to the collisions with $y_c > 0$ and $y_c < 0$.

We describe the orbit by two parameters, a reduced Larmor radius,

$$\rho \equiv (r^2 - \nu^2)^{1/2} - \nu \cos^{-1}(\nu/r) + \nu\pi - \pi/4, \tag{6a}$$

and the phase of the wave,

$$\theta \equiv \nu t \pmod{2\pi}. \tag{6b}$$

(Note that for $r \gg \nu$, $\rho \sim r$.) It is convenient to introduce the sum and difference of these quantities, $v = \theta + \rho$, $u = \theta - \rho$.

Evaluating B_- we note that $\phi_c = -(r_j^2 - \nu^2)^{1/2} - \nu[t_j + \pi - \cos^{-1}(\nu/r_j)] = -v_j - \pi/4$, so that

$$B_- = \alpha(2\pi)^{1/2}(r^2 - \nu^2)^{-1/4} \cos v_j. \tag{7}$$

In (7) we have intentionally dropped the subscripts on r in the amplitude term. The justification for this is that r is large, so a change of order α in r has negligible effect on the amplitude factor compared with the same change in the argument to the cosine.

Working to order α we then find

$$r_{j+1/2} = r_j + (\nu/r)B_-, \tag{8a}$$

$$t_{j+1/2} = t_j + \pi - \frac{(r^2 - \nu^2)^{1/2}}{r^2} B_-, \tag{8b}$$

whence from (6)

$$\rho_{j+1/2} = \rho_j + \nu(r^2 - \nu^2)^{1/2} r^{-2} B_-, \tag{9a}$$

$$\theta_{j+1/2} = \theta_j + \nu\pi - \nu(r^2 - \nu^2)^{1/2} r^{-2} B_- \tag{9b}$$

[note that $\partial\rho/\partial r = (r^2 - \nu^2)^{1/2}/r$], and from (5)

$$u_{j+1/2} = u_j + \nu\pi - 2\pi A \cos v_j, \tag{10a}$$

$$v_{j+1/2} = v_j + \nu\pi, \tag{10b}$$

where

$$A = \left(\frac{2}{\pi}\right)^{1/2} \frac{\alpha\nu(r^2 - \nu^2)^{1/4}}{r^2}. \tag{11}$$

Similarly, we may show that

$$u_{j+1} = u_{j+1/2} + \nu\pi, \tag{12a}$$

$$v_{j+1} = v_{j+1/2} + \nu\pi + 2\pi A \cos u_{j+1}. \tag{12b}$$

Combining (10) and (12) we obtain the following difference equations which give the $(j+1)$th orbit in terms of the jth orbit,

$$u = \theta - \rho, \qquad v = \theta + \rho, \tag{13a}$$

$$\theta = \tfrac{1}{2}(v+u), \qquad \rho = \tfrac{1}{2}(v-u), \tag{13b}$$

$$u_{j+1} - u_j = 2\pi\delta - 2\pi A \cos v_j, \tag{13c}$$

$$v_{j+1} - v_j = 2\pi\delta + 2\pi A \cos u_{j+1}, \tag{13d}$$

where

$$A = \frac{\alpha\nu}{r} \left| H_\nu^{(1)\prime}(r) \right|, \tag{14}$$

$$\delta \equiv \nu - n, \tag{15}$$

$H_\nu^{(1)}$ is the Hankel function of the first kind and of order ν, $|\delta| \le \tfrac{1}{2}$, and n is an integer. In writing (14) we have made use of the expansion of the Bessel functions for $r > \nu + (\tfrac{1}{2}\nu)^{1/3}$ [Ref. 3, Eq. (9.3.3)]. Writing A in this way is mainly a notational convenience, although it comes out naturally in this form when we use the whole cyclotron orbit as the unperturbed orbit.[4] We treat A as being a parameter (independent of ρ) in (13). We shall define T as the mapping which takes a point to its iterate:

$$T(\theta_j, \rho_j) = (\theta_{j+1}, \rho_{j+1}). \tag{16}$$

The limits of validity of (13) are found to be (see Appendix A)

$$\nu \gg 1, \qquad r - \nu \gg (\tfrac{1}{2}\nu)^{1/3}, \qquad A \ll (r^2 - \nu^2)^{3/2}/r^2. \tag{17}$$

Note that the problem now just depends on two parameters, δ and A. This was recognized in I, but was only established analytically in the case $r \gg \nu$, which is much more restrictive than (17).

The difference equations, (13), may be iterated numerically and compared with the solution to the Lorentz force law, (2). Such a comparison is made in Fig. 2, where Fig. 2(a) is taken from I and Fig. 2(b) is obtained from the difference equations. We see that there is excellent agreement, so that the difference equations indeed provide an accurate approximation to the Lorentz force law.

We note that the kicks received by the ions happen at the Landau resonance points (Fig. 1), and so it is interesting to compare the ion motion under the conditions described by (17) with Landau damping in the absence of a magnetic field. There are two important differences. Because the magnetic field sweeps the vector, $\mathbf{v}_\perp$, through all angles, the resonant particles in our case are those for which $r > \nu$ or $v_\perp > \omega/k_\perp$. These particles are much more numerous than those satisfying the normal Landau resonance condition $\dot{y} = \nu$ or $v_y = \omega/k_\perp$. The second difference is that the kick that the particle receives, B, is a function of the magnetic field, since the magnetic field causes the particle to spend only a short time in resonance. In the linear limit of normal Landau damping the resonant particles remain in resonance forever.

III.   SIMPLE PROPERTIES OF THE DIFFERENCE EQUATIONS

The difference equations, (13), describe the mapping of the (θ, ρ) plane onto itself. It models the nonlinear coupling of two harmonic oscillators, the parameter, δ, giving the relation between the unperturbed frequencies and A giving the strength of the coupling. The mapping is area-preserving, being derivable from the generating function,

$$F(u_{j+1}, v_j) = u_{j+1}v_j + 2\pi\delta(u_{j+1} - v_j) + 2\pi A(\sin u_{j+1} + \sin v_j). \tag{18}$$

[Equations (13c) and (13d) are given by $u_j = \partial F/\partial v_j$ and $v_{j+1} = \partial F/\partial u_{j+1}$, respectively.] Thus, (13) describes a Hamiltonian system.

The (θ, ρ) plane is periodic (period 2π) in both the θ and ρ directions and so is topologically equivalent to a $2\pi \times 2\pi$ torus. The periodicity in ρ is a consequence of taking A to be independent of ρ. This, in turn, will allow a very simple determination of the diffusion coefficient (see Secs. VII and VIII). The periodicity in u and v allows a stronger statement to be made, viz., the transformation,

$$\theta \to \theta + \pi, \qquad \rho \to \rho \pm \pi, \tag{19}$$

leaves (13) invariant. This means it is sufficient to examine a range of 2π in θ and π in ρ. Other transformations that leave the difference equations invariant are:

$$\delta \to \delta + 1; \tag{20}$$

$$\delta \to -\delta, \qquad \theta \to \pi - \theta, \qquad \rho \to -\rho; \tag{21}$$

$$A \to -A, \qquad \theta \to \theta - \pi; \tag{22}$$

$$j \to -j, \qquad \theta \to \pi - \theta. \tag{23}$$

The first three of these allow a further restriction of the problem to $0 \leq \delta \leq \frac{1}{2}$ and $A \geq 0$. The last transformation shows the invariance of (13) to time reversal.

IV.   SMALL AMPLITUDE SOLUTION

In this and the next section we examine some aspects of the transition from coherent to stochastic behavior, beginning with the analysis for small A.

It is possible to write down the Hamiltonian for the difference equations, (A13). For small A, canonical transformations similar to those in I may be performed, which allow a solution to the problem. Here we take a different approach which achieves the same results in a more direct manner.

In the limit, $A = 0$, (13) describes two uncoupled harmonic oscillators. If δ is a rational number, s/p, then all the points in the (θ, ρ) plane are pth-order fixed points. If we now let A be small, we expect $\theta_p - \theta_0$ and $\rho_p - \rho_0$ to be small also. In that case the difference equations may be approximated be differential equations for $\dot\theta$ and $\dot\rho$. (It might seem that we are going round in circles here. However, these differential equations will be much simpler than the exact equations of motion, since they describe motion with only one degree of freedom.) If we can find the Hamiltonian, h, such that $\dot\theta = \partial h/\partial\rho$ and $\dot\rho = -\partial h/\partial\theta$, then we have found an additional constant of the motion, h. Lines of constant $h(\theta, \rho)$ give the trajectories of ions in the (θ, ρ) plane.

We begin with the case, $\delta = 0$ (i.e., a cyclotron harmonic). Then (13) becomes

$$u_1 - u_0 = -2\pi A \cos v_0, \tag{24a}$$

$$v_1 - v_0 = 2\pi A \cos u_1 = 2\pi A \cos u_0 + O(A^2), \tag{24b}$$

so that

$$\theta_1 - \theta_0 = 2\pi A \sin \theta_0 \sin \rho_0 + O(A^2), \tag{25a}$$

$$\rho_1 - \rho_0 = 2\pi A \cos \theta_0 \cos \rho_0 + O(A^2). \tag{25b}$$

These equations are Euler's approximation to the solution of the differential equations,

$$\dot{\theta} = A \sin \theta \sin \rho, \tag{26a}$$

$$\dot{\rho} = A \cos \theta \cos \rho. \tag{26b}$$

[We define $\theta_j = \theta(t = 2\pi j)$, etc.] These, in turn, are Hamilton's equations for the Hamiltonian,

$$h = -A \cos \rho \sin \theta. \tag{27}$$

The trajectories of the ion in (θ, ρ) space, given by this Hamiltonian, are shown in Fig. 3(a). This result is the same as that obtained by Timofeev[5] using the full Hamiltonian for the ion. Note that all particles exchange energy with the wave, but that the amount of energy exchanged is bounded in time.

It is instructive to compare this result with standard linear theory. As we noted, our approach is nonlinear because we repeatedly correct the unperturbed orbits. If this is not done (almost) all the orbits are secular with $\rho_N - \rho_0 \sim AN$. These orbits would appear as straight lines in the (θ, ρ) plane which are tangent to the curves drawn in Fig. 3(a) at the initial positions of the ions. Because all the orbits are secular, the linear dielectric function is divergent at a cyclotron harmonic (for $k_\parallel = 0$). Linear theory is valid for $t \lesssim \tau$ where τ is the inverse frequency of motion around the islands in Fig. 3(a). From (27) we find $\tau = A^{-1}$ (near the center of the islands).

For $\delta = \frac{1}{2}$ (i.e., ω at a half harmonic of Ω_i) we find

$$u_2 - u_0 = 2\pi + 4\pi^2 A^2 \sin v_0 \cos u_0 + O(A^3), \tag{28a}$$

$$v_2 - v_0 = 2\pi - 4\pi^2 A^2 \cos v_0 \sin u_0 + O(A^3). \tag{28b}$$

Ignoring the shift of u and v by 2π the differential equations for θ and ρ are

$$\dot{\theta} = \pi A^2 \sin 2\rho, \tag{29a}$$

$$\dot{\rho} = -\pi A^2 \sin 2\theta, \tag{29b}$$

which are derivable from the Hamiltonian,

$$h = -\pi A^2 \cos(\theta + \rho) \cos(\theta - \rho). \tag{30}$$

The trajectories for this case are shown in Fig. 3(b).

The motion is very similar to the case, $\delta = 0$, Fig. 3(a). The most important difference is the extra factor of A in (30) as compared with (27) so that the exchange of energy with

the wave is much slower at a half harmonic. Indeed, to order A there is no exchange of energy since the phase of the ion relative to the wave increases by about π each cyclotron period, and so the kicks received by the ion on successive cyclotron orbits nearly cancel. Thus, there is no contribution to the linear dielectric function from the half harmonics. We expect the $O(A^2)$ change in the speeds of the particles in this case to lead to additional nonlinear terms in the dielectric function which would cause a nonlinear damping of the waves due to half-harmonic resonances.

In the general case where $\delta = s/p \neq 0, \frac{1}{2}$, we have

$$\theta_p - \theta_0 = 2\pi s + p\pi^2 A^2 \frac{\cos(2\rho - \delta\pi)}{\sin(\pi\delta)} + O(A^3), \tag{31a}$$

$$\rho_p - \rho_0 = O(A^3). \tag{31b}$$

These expressions were explicitly checked only for $\delta = \frac{1}{12}, \frac{1}{8}, \frac{1}{6}, \frac{1}{4}, \frac{1}{3}, \frac{3}{8}, \frac{5}{12}$. The algebra required to do the iterations and expansions of the difference equations is quite onerous, and so was performed using the algebraic manipulation system, MACSYMA.[6] We note that the expression for $\dot\theta$ given by dividing (31a) by $2\pi p$ agrees with the expression for the frequencies given by Eq. (43) of I. [This result in I was derived using canonical transformations on the the the Hamiltonian, (A1), and required considerably more effort than (31).] The trajectories in this case are $\rho = \text{const.}$ [Fig. 3(c)]. In this case there is no net exchange of energy between the particles and the wave.

V.   THE STOCHASTIC TRANSITION

For finite A the motion becomes much more complicated. Here we briefly discuss what happens. The exposition is intended to complement that given in I, although there is some overlap. General reviews of the transition to stochasticity may be found in Refs. 7–9.

We begin by noting the topological difference between the cases $\delta = 0, \frac{1}{2}$ and $\delta \neq 0, \frac{1}{2}$ (Fig. 3). This leads to differences in the way that stochasticity develops, and because of this we define the stochasticity threshold differently in the two cases.

With δ not close to 0 or $\frac{1}{2}$, higher-order terms in the difference equations, i.e., the $O(A^3)$ terms in (31), cause islands to appear. The location of the islands may be derived by requiring that $(\theta_p - \theta_0)/(2\pi p)$, (31a), be rational. Where these islands overlap the motion becomes stochastic [Fig. 2(b)]. However, the KAM (Kolmogorov–Arnold–Moser) theorem[10] ensures that for sufficiently small A some trajectories exist which span θ [again see Fig. 2(b)]. [These are KAM "surfaces" reflecting their dimensionality in the original problem, although they only appear as lines in the (θ, ρ) plane.] These act as barriers, preventing ρ for a given particle from increasing or decreasing by more that about π (since the KAM surfaces repeat periodically in ρ). At some value of A the last KAM surface disappears, allowing unrestriced motion in ρ. We define this value of A to be the stochasticity threshold, A_s. In I the value of A_s was found to be about $\frac{1}{4}$. Recently accurate methods for determining A_s have been developed by Greene,[11] although applying these methods to the problem in hand presents difficulties because the relevant resonances do not exist down to $A = 0$.

For δ equal to 0 or $\frac{1}{2}$, we have, for small A, all of phase space covered by islands [Fig. 3(a) and (b)]. When δ is not equal to 0 or $\frac{1}{2}$ but is close to these values, Fig. 3(c) applies only for very small amplitudes. If $A > |\delta|$ or $A > (|1 - 2\delta|/\pi)^{1/2}$, first- and second-order islands appear. At larger amplitudes these islands can cover nearly all of phase space giving

a picture similar to Fig. 3(a) and (b). The effect of finite A in these cases is to produce chains of islands within the main islands. These overlap close to the separatrix causing a layer around the separatrix to become stochastic. For $\delta = 0$ the thickness of this layer is found[12] to be on the order of

$$\exp[-\pi/(2A)] \tag{32}$$

for small A; a similar exponential dependence is expected for $\delta = \frac{1}{2}$. Thus, in contrast with the previous case it is possible for ions to be heated even at low amplitudes. However, for small A, the thickness of the stochastic layer, (32), is extremely small. This means firstly that only a tiny fraction of particles will be in the stochastic region and secondly that those that are will be heated very slowly. Therefore we define the stochasticity threshold in this case as the value of A, A_s, for which the stochastic layer occupies a substantial fraction of phase space. Note that this does not define a precise value of A_s. The definition is useful however since (32) is a strong function of A. In I it was found that A_s had approximately the same value as for $\delta \neq 0$, $\frac{1}{2}$, namely $\frac{1}{4}$.

The stochasticity threshold, $A_s = \frac{1}{4}$, has a simple physical interpretation. At this value of A, the kick received by the particle on one transit through wave-particle resonance (Fig. 1) is sufficient to change the phase that the particle sees when next in wave-particle resonance by $\pi/2$ ($= 2\pi A_s$). This explanation, which is valid for $r > \nu$, complements the explanation in terms of trapping for the case $r \approx \nu$, which was given in I.

We end this section by looking at the eigencurves of the mapping. These are curves in the (θ, ρ) plane which map into themselves on applying the mapping, T. A study of the eigencurves provides another view of the stochastic transition. Again the reader is referred to Refs. 7–9 for a fuller discussion of this. We consider only the case $\delta = 0$. (Because of the additional symmetries in this case, the eigencurves are easier to generate. Similar behavior is observed for other values of δ.) When A is infinitesimal the eigencurves are given by Fig. 3(a); and Fig. 4 shows them for finite values of A. For finite but small A, most of the eigencurves remain closed; these may be generated by iterating the mapping of a single point many times. However, the eigencurves emanating from the hyperbolic fixed points no longer meet up. They are now infinitely long open curves. They are generated as follows: Close to the hyperbolic fixed point, the mapping may be linearized. The eigencurves of the linearized mapping are hyperbolæ. The asymptotes of the hyperbolæ are eigencurves on which a point either moves away from or towards the fixed point. These eigencurves are called the unstable and stable manifolds respectively. Short straight line segments, which connect a point with its image under T, are chosen on these unstable and stable manifolds. These line segments are then repeatedly mapped forwards and backwards by applying T and T^{-1}; and the union of the mapped segments generates the open eigencurves. In practice, only a few (less than 10) iterations are required. Figure 4(a) shows the eigencurves for $A = 0.3$. We see that the open curves intersect each other at a finite angle, and start oscillating as they approach the fixed point. Because the mapping is area-preserving these oscillations grow larger and larger as the fixed point is approached. These curves occupy a finite area which may be shown to be stochastic. As illustration of this we show the iteration of a single point starting close to the hyperbolic fixed point (Fig. 5). We see that it covers nearly all the area outside the first-order islands. All these points lie on a single eigencurve. The area occupied by the eigencurves (i.e., the area of phase space that is stochastic) is proportional to the angle at which the eigencurves first intersect (approximately half way between the fixed points). This then gives another way, in addition to the method of island overlap, of estimating the fraction of phase space that is stochastic. This angle again has

the exponential dependence on amplitude given in (32). In Fig. 4(b), A has been increased to 0.35. Here we see the open eigencurves intersecting at a larger angle. In addition, the elliptic fixed points in Fig. 4(a) have turned into hyperbolic fixed points with reflection [from (B7) we find that this happened at $A = \pi^{-1} \approx 0.318$]. Thus, open eigencurves emanate from these points. However, the angle at which they intersect is so small that the area they occupy is comparable to the thickness of the lines used to draw the figure. Eigencurves corresponding to the original islands are still present. However, these have disappeared at $A = 0.45$, Fig. 4(c). At this amplitude the two sets of open eigencurves intersect each other. This may be seen by comparing this figure with Fig. 4(d), where we have extended one of the eigencurves emanating from the hyperbolic fixed point with reflection.

VI. THE KRYLOV–KOLMOGOROV–SINAI ENTROPY

Having established that the ion motion becomes stochastic for $A > A_s$, we need to be able to describe the motion above the stochasticity threshold. One of the most important parameters in this regard is the Krylov–Kolmogorov–Sinai (KS) entropy, h. This is a measure of the local instability of trajectories and is defined as the average rate of divergence of neighboring (infinitely close) trajectories. Thus, after N iterations the distance between neighboring particles initially d_0 apart is approximately $d_0 \exp(hN)$ (for d_0 small and N large).

The KS entropy is important for two reasons. Firstly, given a group of particles which initially occupy a small region of phase space, $\Delta\theta \, \Delta\rho$, we can estimate the number of iterations for the phases, θ, of the particles to become random to be

$$\log(2\pi/\Delta\theta)/h. \tag{33}$$

Secondly, the exponential divergence of trajectories leads to a *mixing* of phase space, which in turn results in the decay of the correlation function, C_k (Sec VII), and allows the motion of the particle to be described by a diffusion equation.

In order to determine h we define a reference trajectory, (u_j, v_j). [It is more convenient to work in (u, v) space.] We consider a neighboring trajectory, $(u_j + \delta u_j, v_j + \delta v_j)$, where δu_j and δv_j are infinitesimals. Then δu_j and δv_j satisfy

$$\begin{pmatrix} \delta u_{j+1} \\ \delta v_{j+1} \end{pmatrix} = \mathbf{J}_j \begin{pmatrix} \delta u_j \\ \delta v_j \end{pmatrix}, \tag{34}$$

where

$$\mathbf{J}_j \equiv \begin{pmatrix} 1 & 2\pi A \sin v_j \\ -2\pi A \sin u_{j+1} & 1 - 4\pi^2 A^2 \sin u_{j+1} \sin v_j \end{pmatrix}. \tag{35}$$

If we define $\mathbf{M}_N$ by

$$\mathbf{M}_N = \prod_{j=0}^{N-1} \mathbf{J}_j, \tag{36}$$

then h is given by

$$h = \lim_{N \to \infty} (\log|\Lambda_N|/N), \tag{37}$$

where Λ_N is the largest (in magnitude) eigenvalue of $\mathbf{M}_N$. This definition is equivalent to[9]

$$h = \langle \log(\ell_{j+1}/\ell_j) \rangle, \tag{38}$$

where ℓ_j is the length of the vector $(\delta u_j, \delta v_j)$ and the average is taken over a particle orbit.

Figure 6 shows $\log|\Lambda_N|/N$ as a function of n for various values of A. We see that it does have a limiting value as $N \to \infty$ and so h is well defined. Figure 7 shows h as a function of A for $\delta = 0.23$. For A small, h is close to zero, because when the motion is coherent neighboring trajectories diverge linearly, rather than exponentially. When A is still below A_s, h becomes finite, since the reference trajectory was chosen in the stochastic part of phase space (Fig. 2). As A passes through the stochasticity threshold there is a slight drop in h. Finally, for $A \gg A_s$, h is on the order of $\log A$.

We may derive the expression for h in the limit $A \gg A_s$. If λ_j and μ_j are the larger and smaller (in magnitude) eigenvalues of $\mathbf{J}_j$, then for $A \gg A_s$ we have

$$\lambda_j \approx -4\pi^2 A^2 \sin u_{j+1} \sin v_j, \qquad \mu_j = 1/\lambda_j. \tag{39}$$

Furthermore, the eigenvectors corresponding to these eigenvalues are approximately $\hat{\mathbf{v}}$ and $\hat{\mathbf{u}}$ respectively. Since the eigenvectors for different $\mathbf{J}_j$ are nearly parallel to one another, the eigenvalues of the product of the $\mathbf{J}_j$ are approximately the product of the eigenvalues of the $\mathbf{J}_j$; i.e.,

$$\Lambda_N \approx \prod_{j=0}^{N-1} \lambda_j. \tag{40}$$

Substituting (39) into (40) we have

$$h = \langle \log|\lambda_j| \rangle = 2\log(\pi A) + \langle \log|4 \sin u_{j+1} \sin v_j| \rangle, \tag{41}$$

where the average is taken over a particle orbit. Finally, we note that for $A \gg A_s$, a particle's orbit wanders over most of phase space, spending equal amounts of time in equal areas of phase space (i.e., the particle's orbit is approximately ergodic). Thus, the average along the orbit may be replaced by a phase space average. The last term in (41) becomes

$$2(2\pi)^{-1} \int_0^{2\pi} \log|2 \sin \psi| \, d\psi = 0 \tag{42}$$

[see Ref. 3, Eq. (4.3.145)]. Thus, for $A \gg A_s$, we have

$$h \approx 2\log(\pi A). \tag{43}$$

This is shown as a dashed line in Fig. 7.

VII.   THE CORRELATION FUNCTION

We saw in the last sections that a group of particles initially close together in phase space separate exponentially. This continues until a time on the order of h^{-1}, (33). After this time the phase of the particles may take on any values. We wish to ascertain the behavior of the particles for longer times. More precisely, if we consider an ensemble of particle trajectories, (θ_j, ρ_j), then what are the moments, $\langle \rho_N - \rho_0 \rangle$, $\langle (\rho_N - \rho_0)^2 \rangle$, for large N? (The brackets denote ensemble averages.)

Firstly, let us consider the average force on the ensemble,

$$f \equiv \frac{\langle \rho_N - \rho_0 \rangle}{N}. \tag{44}$$

By shifting the origin of time by N (which leaves the difference equations invariant) we have

$$f = \frac{\langle \rho_0 - \rho_{-N} \rangle}{N},$$ (45a)

and by reflecting time using the symmetry, (23), we have

$$f = \frac{\langle \rho_{-N} - \rho_0 \rangle}{N}.$$ (45b)

From (45a) and (45b) we see that $f = 0$.

Turning to the second moment, we first define an acceleration.

$$a_j = \rho_{j+1} - \rho_j.$$ (46)

(In defining a_j, we do *not* treat ρ as a periodic variable.) Then we have

$$\langle (\rho_N - \rho_0)^2 \rangle = \sum_{i=0}^{N-1} \sum_{j=0}^{N-1} \langle a_i a_j \rangle.$$ (47)

We define a correlation function, C, by

$$C\left(\frac{i+j}{2}, i-j \right) = \langle a_i a_j \rangle.$$ (48)

C has the following properties:

$$C(\ell, k) = C(0, k) \equiv C_k,$$ (49a)

which follows from the invariance of the system to a shift in the origin of time, and

$$C_k = C_{-k},$$ (49b)

since $\langle a_i a_j \rangle = \langle a_j a_i \rangle$. Because of (49a) the definition of C_k may include an average over a single orbit, as well as an ensemble average. [We will usually use a subscript, N, to denote the time (i.e., the iteration number), while a subscript, k, will denote a time difference.]

Rewriting (47) in terms of C_k and using properties, (49), we find

$$\langle (\rho_N - \rho_0)^2 \rangle = NC_0 + \sum_{k=1}^{N-1} 2(N-k)C_k.$$ (50)

For $N \to \infty$ we have

$$\langle (\rho_N - \rho_0)^2 \rangle = 2\mathcal{D}N,$$ (51)

where the diffusion coefficient, $\mathcal{D}$, is given by

$$\mathcal{D} = \frac{1}{2}C_0 + \sum_{k=1}^{\infty} C_k$$ (52)

and we have assumed that C_k decays sufficiently rapidly so that the sum in (52) exists.

In order to find C_k numerically we compute M orbits of length, L. Then C_k is approximated by

$$C_k = (L - k + 1)^{-1} \sum_{\ell=0}^{L-k} \langle a_\ell a_{\ell+k} \rangle,$$ (53)

where the average is now over the M orbits.

Figure 8 shows examples of the correlation function for $\delta = 0.23$ and various values A. When $A < A_s$, Fig. 8(a), C_k is highly oscillatory, and decays slowly. As A is increased above the stochasticity threshold, the correlation time, k_c, rapidly decreases, Fig. 8(b), becoming approximately 0 for $A \gtrsim 1$, Fig. 8(c).

Note that in defining the ensemble of orbits we did not specify what ρ_0 was, so that different members of the ensemble could have different values of ρ_0. Because of the periodicity of the difference equations, (13), in ρ, we know that $\rho_0 \pmod{2\pi}$ is sufficient to determine $\rho_N - \rho_0$. Thus, the ensemble average provides an average of the initial conditions over an interval of 2π, which is of little consequence. Averaging along a given orbit (for $A > A_s$) has the same effect. Having performed this averaging, C_k is independent of ρ.

The situation is much more complicated in the original system described by the Lorentz force law, (2). In that case the problem is not periodic in r, since A has a slow dependence on r, (14). Now, we would be hiding this important dependence on r if we did not restrict the starting positions of the orbits, r_0. Similarly, we could not perform the averaging along the orbit. Thus, C_k becomes a function of r, and it is more difficult to compute, since less averaging can be done. Finally, the diffusion coefficient would be more difficult to define because, although $\langle (r_N - r_0)^2 \rangle$ might be proportional to N for some range of N, it certainly will not be proportional to N for large N, since the particles will be coming into regions where A and C_k are different.

These problems are all circumvented by using the difference equations. These allow a simple and rapid determination of C_k and $\mathcal{D}$. The dependence of the diffusion coefficient on r will be recovered through its dependence on A (Sec. IX).

VIII.   THE DIFFUSION COEFFICIENT

We now turn to the diffusion coefficient for the ions. We shall use (52) to define and calculate $\mathcal{D}$. In the limit $A \gg A_s$ we can obtain an estimate for $\mathcal{D}$ based on the observation of the last section that the correlation time is short in this limit, viz., $C_k = 0$ for $|k| > 0$ [see Fig. 8(c)]. In this case we have $\mathcal{D} = \frac{1}{2} C_0$, with $C_0 = \langle a_0^2 \rangle$, where the average is taken over an ensemble and down a trajectory. In the same spirit that we calculated the KS entropy, h, in the limit $A \gg A_s$ (Sec. VI), we shall assume that the ion trajectories are ergodic so that the ensemble and trajectory averages may be replaced by a phase space average. Thus, we obtain

$$
\begin{aligned}
\mathcal{D} = \tfrac{1}{2}\langle a_0^2 \rangle &= \tfrac{1}{8}\langle [(v_1 - v_0) - (u_1 - u_0)]^2 \rangle \\
&= \tfrac{1}{2}\pi^2 A^2 \langle (\cos u_1 + \cos v_0)^2 \rangle \\
&= \pi^2 A^2 (2\pi)^{-1} \int_0^{2\pi} \cos^2 \psi \, d\psi \\
&= \tfrac{1}{2}\pi^2 A^2.
\end{aligned}
\tag{54}
$$

When A is not large we expect the presence of islands to obstruct the diffusion of ions leading to a value of $\mathcal{D}$ below (54). [This is reflected in the correlation function by the fact that for small k, $C_{k>0} < 0$; see Fig. 8(b).] Finally, for $A < A_s$ diffusion is stopped. (Strictly speaking this only happens when δ is not close to 0 or $\frac{1}{2}$, for then there are KAM surfaces

preventing the diffusion of ions. However, as discussed in Sec. V, the diffusion for $A < A_s$ for δ close to 0 or $\frac{1}{2}$ is extremely slow.) We therefore expect $\mathcal{D}$ to have the form,

$$\mathcal{D} = \tfrac{1}{2}\pi^2 A^2 g^2(A), \tag{55}$$

where $g(A) \leq 1$, $g(|A| \to \infty) \to 1$, and $g(|A| < A_s) = 0$.

We test these ideas out by numerically finding $\mathcal{D}$, and hence $g(A)$, for various values of δ. We determine $\mathcal{D}$ by first finding C_k using (53) and then computing

$$\mathcal{D} = \tfrac{1}{2}C_0 + \sum_{k=1}^{K} q_k C_k, \tag{56a}$$

where q_k is a windowing function given by

$$q_k = \begin{cases} 1, & \text{for } 0 < k \leq K', \\ \dfrac{1}{2}\left[1 + \cos\left(\pi \dfrac{k - K'}{K + 1 - K'}\right)\right], & \text{for } K' < k \leq K. \end{cases} \tag{56b}$$

The reason for introducing a windowing function into (56) is to suppress the effect of the oscillations seen in Fig. 8(a). Criteria for choosing K and K' are $K - K' \gg 1$ for $A < A_s$ (in order to suppress the oscillations in C_k), $K' \gg k_c$ for $A > A_s$ (so as to include the major contribution to $\mathcal{D}$), and finally $K \ll L$, where L is the length of the orbits used to calculate C_k, (53). This last condition arises because, from (53), the number of samples entering into C_k is $M(L-k+1)$ which we wish to be large in order to suppress the statistical fluctuations in C_k.

Note that if we had computed $\mathcal{D}$ directly by measuring $(\rho_L - \rho_0)^2$ for M orbits, there would be only M samples contributions to $\mathcal{D}$. Thus, the error in $\mathcal{D}$ would be $O(M^{-1/2})$. When computing $\mathcal{D}$ using C_k we effectively include all possible shorter orbits that make up the orbit ρ_0 to ρ_L. There are about L/k_c independent orbits in an orbit of length, L. The error in $\mathcal{D}$ is then $O[(k_c/ML)^{1/2}]$ which can be much less than the error when computing $\mathcal{D}$ directly.

Figure 9 shows $g(A)$ for three value of δ. Although g has the general form discussed earlier, there are some anomalies. Instead of approaching unity monotonically as $A \to \infty$, there is a tendency for g to oscillate about unity with a period of unity in A. This is particularly noticeable with δ equal to 0.11 and 0.47. The oscillations are about $\pm 20\%$ for $1 \leq A \leq 2$ and about $\pm 10\%$ for $20 \leq A \leq 22$. Also there is a very strong peak in $g(A)$ for $\delta = 0.47$ and $A = 0.55$. Both these phenomena are due to the existence of "accelerator" modes, or island systems for which the ion, rather than returning to its original island, returns to an island displaced upwards or downwards in ρ by an integer multiple of π.

Some of these accelerator modes are studied in Appendix B. From (B4) with $m = 1$ and $n = 0$ we find that there exists a stable accelerating fixed point for $\delta = 0.47$ and $0.53 < A < 0.5971$. So for $A = 0.55$ there are orbits in the island system for which $\rho_N \sim \pm\pi N$. Although the orbits used to calculate $\mathcal{D}$ all lay outside this island system, they could wander close to the island and become temporarily trapped close to the island (for up to several hundred iterations). This results in a very slow decay of the correlation function (Fig. 10), and an anomalously high diffusion coefficient.

As A is increased, a new set of accelerator modes appear at values of A equal to $p \pm \delta$, where p is an integer. The islands disappear by becoming unstable, shortly afterwards. This leads to the oscillatory behavior in $\mathcal{D}$ seen in Fig. 9. Similar oscillation have been observed

by Chirikov[9] for the so-called standard mapping. He also associated these oscillations with the presence of accelerator modes.

In our case there are probably no accelerator modes present in the cases for which $g(A)$ is plotted in Fig. 9 (except the case previously discussed, i.e., $\delta = 0.47$, $A = 0.55$). The oscillations may however arise from the unstable fixed points that remain after the islands turn unstable. Such unstable fixed points may marginally increase the correlation time and hence the diffusion coeficient. As δ is increased these fixed points become more unstable and the effect is diminished. Choosing A in the small windows where the accelerator modes exist would have given peaks in $g(A)$ similar to the one at $\delta = 0.47$ and $A = 0.55$. We may argue that the peaks in $g(A)$ that occur when the accelerator modes are present are unphysical. In Appendix B we establish that the window in A for which these modes exist is quite narrow. Now, as an ion is being accelerated or decelerated by one of these modes, ρ and r, (6a), will be changing. Hence, after a while we must recognize that A, which is a function of r, (14), will also change. This will "switch off" the accelerator modes after only a few iterations, and the correlation times will similarly be limited. The effect of the slow change of A (which was ignored in deriving the difference equations) will be to remove the peaks in $g(A)$, leaving only the gentle decaying oscillations in $g(A)$.

For these reasons $g(A)$ was fitted by the simplest smooth curve that reasonably fits the data. Figure 9 shows the functional form chosen, viz.,

$$g(A) = \max\left(\frac{A^2 - A_s^2}{A^2}, 0\right), \tag{57}$$

with $A_s = \frac{1}{4}$. This form of g will be checked in the next section by solving the resulting diffusion equation, and comparing the results with the solution of the exact equations of motion, (2).

IX.   DERIVATION OF A DIFFUSION EQUATION

With $A > A_s$ we expect the distribution, $f(\rho, N)$, of a group of ions after N iterations to spread according to a diffusion equation. We will briefly outline the arguments that lead to this result.

Suppose m is greater than the correlation time, k_c, and let us look at the results of the mapping only at times, N, which are an integer multiple of m. Then the mapping, T, may be approximated by a Markovian process, which is described by a transition probability, $P(\rho_1 \mid \rho_2, N)\, d\rho_2$, which is the probability the a particle is found in the range, $(\rho_2, \rho_2 + d\rho_2)$, given that it was at ρ_1, N iterations earlier. P must satisfy

$$P(\rho_1 \mid \rho_2, N) = \int d\rho\, P(\rho_1 \mid \rho, k) P(\rho \mid \rho_2, N - k) \tag{58}$$

for all k such that k is a multiple of m and $0 < k < N$.

For long times f will be spread over several periods in ρ. In that case we are not interested in the details of f that occur over the period, 2π, in ρ. We retain the important physical effects when we average f and P over a period in ρ. (Precisely this averaging is carried out in computing C_k and $\mathcal{D}$ in Secs. VII and VIII.) In that case P only depends on the difference, $\rho_2 - \rho_1$, and we have

$$P(\rho_1 \mid \rho_2, N) = P(\rho_2 - \rho_1, N). \tag{59}$$

The evolution of the distribution of ions, f, is given by

$$f(\rho, N) = \int d\rho_1 \, f(\rho_1, N_1) P(\rho - \rho_1, N - N_1). \tag{60}$$

The moments of P,

$$a_n(N) \equiv \int d\rho \, \rho^n P(\rho, N), \tag{61}$$

are the same as the moments, $\langle (\rho_n - \rho_0)^n \rangle$, studied in Sec. VII. Thus, we have

$$a_1(N)/N = 0, \tag{62a}$$

$$a_2(N)/N = 2\mathcal{D}, \tag{62b}$$

for $N \geq m$.

Following the analysis of Chandrasekhar[13] and Wang and Uhlenbeck[14] we may use (58) to derive a Fokker–Planck equation for the evolution of P for $N \gg k_c$:

$$\frac{\partial P}{\partial N} = \frac{\partial^2}{\partial \rho^2} \mathcal{D} P. \tag{63}$$

Substituting for f from (60) gives

$$\frac{\partial f}{\partial N} = \frac{\partial}{\partial \rho} \mathcal{D} \frac{\partial}{\partial \rho} f, \tag{64}$$

where we have used the result that $\mathcal{D}$ is independent of ρ in order to write the diffusion equation in its more usual form. Incidentally, although we derived (64) for $A > A_s$ it clearly gives satisfactory results for $A < A_s$, because g and $\mathcal{D}$ are then zero, and f does not evolve.

We now undo the normalizations made earlier. Writing $N = t/2\pi$ and converting ρ to r using (6a) we have

$$\frac{\partial f}{\partial t} = \frac{1}{r} \frac{\partial}{\partial r} r \frac{\mathcal{D}}{2\pi} \left(\frac{\partial \rho}{\partial r} \right)^{-2} \frac{\partial}{\partial r} f, \tag{65}$$

where $\partial \rho / \partial r = (r^2 - \nu^2)^{1/2}/r = \left| H_\nu^{(1)\prime}(r) / H_\nu^{(1)}(r) \right|$ for $r > \nu + (\frac{1}{2}\nu)^{1/3}$. In writing (65) in this form we have replaced the first derivative operator in (64) by the cylindrical divergence operator, in order to ensure conservation of particles. (The normalization of f is such that $\int dv_\parallel \int dr \, 2\pi r f = 1$. We will suppress the dependence of f on the velocity parallel to $\mathbf{B}$, $v_\parallel$, until we consider the effects of collisions in Secs. X–XII.) Note that $\mathcal{D}$ is now a function of r through A, i.e., $\mathcal{D} = \mathcal{D}[A(r)]$, so that we must justify our commuting $\mathcal{D}$ with the second derivative operator between (63) and (64). The argument for having $\mathcal{D}$ where it is in (65) is that in the steady state f should be a constant in the stochastic region. This is a result of the approximate ergodicity of the motion, when described by the exact equations of motion, (2), and was observed in the simulation described in I. We shall presently compare the results obtained by the diffusion equation with that simulation. Rewriting (65) using (55) and (14) we obtain

$$\frac{\partial f}{\partial t} = \frac{1}{r} \frac{\partial}{\partial r} r D \frac{\partial}{\partial r} f, \tag{66}$$

where

$$D(r) = \frac{\mathcal{D}}{2\pi} \left(\frac{\partial \rho}{\partial r} \right)^{-2} = \frac{\pi}{4} \left(\frac{\alpha \nu}{r} \left| H_\nu^{(1)}(r) \right| g(A) \right)^2 \tag{67a}$$

for $r \geq \nu$. We extend the definition of D to $r < \nu$ as follows:

$$D(r) = \begin{cases} D(\nu), & \text{for } \nu - \sqrt{\alpha} \leq r < \nu, \\ D(\nu)[r - (\nu - 2\sqrt{\alpha})]^2/\alpha, & \text{for } \nu - 2\sqrt{\alpha} \leq r < \nu - \sqrt{\alpha}, \\ 0, & \text{for } r < \nu - 2\sqrt{\alpha}. \end{cases} \tag{67b}$$

When numerically computing D we use the approximate forms for H and H',

$$\left| H_\nu^{(1)}(r) \right| \approx (2/\pi)^{1/2}(r^2 - \nu^2)^{-1/4}, \tag{68a}$$

$$\left| H_\nu^{(1)\prime}(r) \right| \approx (2/\pi)^{1/2}(r^2 - \nu^2)^{1/4}/r, \tag{68b}$$

for $r \geq \nu + (\frac{1}{2}\nu)^{1/3}$ and

$$\left| H_\nu^{(1)}(r) \right| \approx \left| H_\nu^{(1)}[\nu + (\frac{1}{2}\nu)^{1/3}] \right|, \tag{68c}$$

for $\nu \leq r < \nu + (\frac{1}{2}\nu)^{1/3}$ and similarly for H'. We will show the typical form of D in Sec. XI.

Because of the restrictions on r in the derivation of the difference equations (Sec. II), we must justify (67) for $r < \nu + (\frac{1}{2}\nu)^{1/3}$. In this range, the choice of the form of D is motivated by the following considerations: Firstly, in the region, $\nu - \sqrt{\alpha} < r < \nu + (\frac{1}{2}\nu)^{1/3}$ trapping[4] plays a dominant rôle. This trapping is similar to the trapping of a particle by a wave in the absence of a magnetic field and its effect is to cause a rapid mixing of f in this region. This is modeled by (67) since D is approximately constant and has its maximum value in this region. Secondly, we find that particles are fed quite slowly into the trapping region from below and this is given by the form of D for $\nu - 2\sqrt{\alpha} < r < \nu - \sqrt{\alpha}$. Finally, the motion is coherent for $r < \nu - 2\sqrt{\alpha}$ in which case D is 0.

In order to check (66) and (67) we compare the results obtained using these equations with the results of the simulation described in I. In the latter case the orbits of 50 particles were found by integrating the exact equations of motion, (2). Because of the small number of particles involved the comparison is most easily made if we solve (66) using a simple Monte Carlo method described in Appendix C. It might seem as though we are back-tracking here, by going back to difference equations. However, the Monte Carlo method for (66) differs from the original equations, (13), in two respects: firstly, the randomness is explicitly inserted; and, secondly, we allow for the variation of D with r. This latter aspect of the solution we present here allows us to justify the placement of D with respect to the derivative operators in (66). Figures 11 and 12 show the comparison. In each case we follow the motion of $N = 50$ particles with initial perpendicular velocities, $r_0 = 23$, and with $\alpha = 20$, $\nu = 30.23$. The general features of these figures are discussed in I. For our purposes we see that there is good agreement between the two simulations. In particular, note the agreement in the short time behavior, Fig. 11(c) and (d), and in the averaged distribution function, Fig. 12. These two points respectively confirm the form taken for D for $r \lesssim \nu$ in (67b) and the placement of D with respect to the derivative operators in (66). We conclude that (66) with D given by (67) accurately models the diffusion of ions in the presence of a perpendicularly propagating electrostatic wave.

We may write D in dimensional form by multiplying (67) by $\Omega_i^3/k_\perp^2$ to give

$$D(v_\perp) = \begin{cases} \dfrac{\pi}{4} \dfrac{(E_0/B_0)^2 \omega^2 \Omega_i}{k_\perp^2 v_\perp^2} \left|H_\nu^{(1)}(r)\right|^2 g^2(A)\gamma, & \text{for } v_\perp \geq v_{\text{ph}}, \\[2ex] D(v_{\text{ph}}), & \text{for } v_{\text{ph}} - v_{\text{tr}} \leq v_\perp < v_{\text{ph}}, \\[2ex] D(v_{\text{ph}})[v_\perp - (v_{\text{ph}} - 2v_{\text{tr}})]^2/v_{\text{tr}}^2, & \text{for } v_{\text{ph}} - 2v_{\text{tr}} \leq v_\perp < v_{\text{ph}} - v_{\text{tr}}, \\[2ex] 0, & \text{for } v_\perp < v_{\text{ph}} - 2v_{\text{tr}}, \end{cases} \tag{69}$$

where $g(A)$, ν, and r are given by (57), (14), and (3), $v_{\text{ph}} = \omega/k_\perp$, and v_{tr} is the trapping velocity,

$$v_{\text{tr}} = (q_i E_0/m_i k_\perp)^{1/2}. \tag{70}$$

In (69) we have included an additional factor, γ, which is defined as the fraction of time that the ion orbits spend in the region of lower hybrid waves. This reflects the fact that the ion can only diffuse a fraction, γ, of the time. In order to include the spatial variation of the lower hybrid waves in such a simple way, two conditions must be satisfied. The ions must spend many cyclotron periods in the lower hybrid waves, so that the difference equations are applicable, and the motion is described by (64). The opposite limit, where the ion spends a small fraction of a cyclotron period in the wave, has been considered by Lazarro[15] in the context of heating a fast beam of ions. Secondly, we must be able to model the lower hybrid wave as a product of a single **k** component and a square-wave envelope. The first condition is usually satisfied in cases of practical interest and, because the lower hybrid waves travel in well-defined rays,[16] the second condition is also normally satisfied. In cases where the envelope of the lower hybrid waves is not a square wave, the definition of D, (69), may be replaced by the average of (69), without the factor, γ, over the ion's orbit. For a circulating ion in a tokamak which covers a magnetic surface ergodically, γ is approximately the ratio of the area of the intersection of the lower hybrid ray with the magnetic surface to the total area of the magnetic surface. This ignores the finite extent of the lower hybrid wave in the perpendicular direction. When this is included, γ is reduced since the cyclotron orbit must be completely in the lower hybrid ray for the difference equations, (13), to hold. The diffusion equation for the ions written in unnormalized form becomes

$$\frac{\partial f}{\partial t} = \frac{1}{v_\perp} \frac{\partial}{\partial v_\perp} v_\perp D \frac{\partial}{\partial v_\perp} f. \tag{71}$$

In the next sections we study the properties of this equation when we add a Fokker–Planck collision term.

X.   INCLUSION OF COLLISIONS

We have seen that the ions can irreversibly exchange energy with the wave. However, because $\omega/k_\perp$ is usually several times the ion thermal speed, only the tail ions are affected. Bulk heating only takes place when these ions collide with the background. We investigate this process by including a Fokker–Planck collision term in (71) to give

$$\frac{\partial f}{\partial t} = \frac{1}{v_\perp} \frac{\partial}{\partial v_\perp} v_\perp D \frac{\partial}{\partial v_\perp} f + \left(\frac{\partial f}{\partial t}\right)_c. \tag{72a}$$

Since only a relatively few tail particles are affected by the wave we can neglect the tail-tail collisions when determining $(\partial f/\partial t)_c$. We can thus linearize this term by assuming the the background distributions of ions and electrons are Maxwellians. We then obtain[17]

$$(\partial f/\partial t)_c = -\sum_\beta \nabla \dot{\mathbf{J}}^{i/\beta}, \tag{72b}$$

where β is a species label (i or e),

$$-\mathbf{J}^{\alpha/\beta} = \frac{m_\alpha}{m_\alpha + m_\beta}\nu_s^{\alpha/\beta}\mathbf{v}f_\alpha + \frac{1}{4}\nu_\perp^{\alpha/\beta}v^2\nabla_{\mathbf{v}}f_\alpha$$

$$+ \left(\frac{1}{2}\nu_\parallel^{\alpha/\beta} - \frac{1}{4}\nu_\perp^{\alpha/\beta}\right)\mathbf{v}\mathbf{v}\dot{\nabla}_{\mathbf{v}}f_\alpha, \tag{72c}$$

and expressions for the collision frequencies, ν, can be found in Ref. 18.

   We next simplify (72) by reducing it to a problem in only one velocity dimension, $v_\perp$, by integrating (72a) over $v_\parallel$. The procedure we follow for doing this is very similar to that employed by Fisch[19,20] to derive a one-dimensional Fokker–Planck operator in $v_\parallel$ in order to study rf-driven currents. When performing the integral over $v_\parallel$ the term involving $J_\parallel^{\alpha/\beta}$ drops out. We then need only to evaluate $-\int dv_\parallel\, J_\perp^{i/\beta}$. In order to do this we make three assumptions: Firstly, we assume that $f\ (= f_i)$ has the form,

$$f(v_\perp, v_\parallel) = F(v_\perp)(2\pi T_i/m_i)^{-1/2}\exp(-\tfrac{1}{2}m_iv_\parallel^2/T_i); \tag{73}$$

i.e., the dependence of f on $v_\parallel$ is that of a Maxwellian. Secondly, we assume that $v_\perp^2 \gg T_i/m_i$. This allows us to replace v by $v_\perp$ in the expressions for the collisions frequencies, so that they drop out of the integral. Lastly, we assume that the background temperatures are all equal so that $T_\beta = T_i$. (Without this assumption additional sources and sinks of energy are required to maintain an equilibrium.) Then we have

$$-\int dv_\parallel\, J_\perp^{i/\beta} = C_\beta\, \partial F/\partial v_\perp + (m_iv_\perp/T_i)C_\beta F + O[T_i/(m_iv_\perp^2)], \tag{74}$$

where

$$C_\beta = \tfrac{1}{2}\nu_\parallel^{i/\beta}v_\perp^2 + \tfrac{1}{4}\nu_\perp^{i/\beta}T_i/m_i, \tag{75}$$

and we have used[18]

$$\frac{m_\alpha}{m_\alpha + m_\beta}\nu_s^{\alpha/\beta} = \frac{m_\alpha v^2}{T_\beta}\frac{1}{2}\nu_\parallel^{\alpha/\beta}. \tag{76}$$

Substituting these results into the integral of (72a) over $v_\parallel$ gives

$$\frac{\partial F}{\partial t} = \frac{1}{v_\perp}\frac{\partial}{\partial v_\perp}v_\perp\left[D\frac{\partial F}{\partial v_\perp} + C\left(\frac{\partial F}{\partial v_\perp} + \frac{v_\perp}{v_{ti}^2}F\right)\right], \tag{77}$$

where $C = \sum_\beta C_\beta$ and $v_{ti}^2 = T_i/m_i$. If $D = 0$, we recover a Maxwellian for F. Thus, we shall use (77) to solve for F for all $v_\perp$ even though it was derived only in the high velocity limit. We expect that this will not entail much additional error as long as D is finite only where $(v_\perp/v_{ti})^2$ is large.

XI.   NUMERICAL SOLUTION OF FOKKER–PLANCK EQUATION

A number of approximations need to be made in the derivation of the one-dimensional Fokker–Planck equation, (77). These leave the accuracy of (77) open to question. In particular the factorization of f by (73) is not easy to rigorously justify. In this section we compare the numerical solutions of the one-dimensional and two-dimensional Fokker–Planck equations, (77) and (72). A similar, but more extensive, comparison has been carried out[21] for the parallel one-dimensional Fokker–Planck equation for the electrons with a parallel quasilinear diffusion term, derived by Fisch.[19,20] For reasons that we will discuss we expect better agreement in the present case. Therefore, we content ourselves with presenting here the solution for one particular case.

Consider a hydrogen plasma with ion density, $n_0 = 10^{20}$ m^{-3}, magnetic field, $B_0 = 4$ T, and temperature, $T_e = T_i = 2$ keV. Let the lower hybrid wave be described by $\omega/(k_\perp v_{ti}) = 3.5$, $\omega/\omega_{lh} = 1.3$, and $E_0 = 10^6$ V/m. The frequency of such a wave is 2.13 GHz. Its parallel wavenumber may be found by solving the dispersion relation $K_\parallel k_\parallel^2 + K_\perp k_\perp^2 - 3(\omega_{pi}^2 v_{ti}^2/\omega^4)k_\perp^4 = 0$, where $K_\parallel$ and $K_\perp$ are elements of the cold plasma dielectric tensor. This gives $\omega/(k_\parallel v_{te}) = 5.25$ and a parallel index of refraction, $n_\parallel = 3.06$. This wave represents a typical Fourier component of a lower hybrid wave near the center of the tokamak, but before it has reached the point of thermal wave conversion. Note that, because of the high value of $\omega/(k_\parallel v_{te})$, we expect electron Landau damping to be negligible. The normalized parameters are then found from (3) to be $\nu = 35$, $\alpha = 5.71$. We take the extent of the lower hybrid ray in the parallel direction to be $\Delta z = 0.4$ m, the major radius of the tokamak to be $R = 2$ m, and the angular extent of the wave in the poloidal direction to be $\Delta\theta = \pi/4$. The geometrical factor, γ, appearing in (69) is given by

$$\gamma \approx \frac{\Delta z}{2\pi R} \frac{\Delta\theta}{2\pi} = \frac{1}{251}. \tag{78}$$

[As discussed in Sec. IX, this value of γ should be slightly reduced to account for the finite perpendicular extent of the waves. However, (78) is sufficiently accurate for illustrative purposes.] Substituting these values into D, (69), at $v_\perp = \omega/k_\perp$ gives

$$D(\omega/k_\perp) = 1.5\, v_{ti}^2 \nu_0^{i/i}, \tag{79}$$

where we have written D in terms of a collisional diffusion coefficient $v_{ti}^2 \nu_0^{i/i}$ and $\nu_0^{i/i}$ is the ion collision frequency for thermal particles

$$\nu_0^{i/i} = \frac{\lambda_{ii}\omega_{pi}^4}{4\pi n_0 v_{ti}^3}. \tag{80}$$

We take the Coulomb logarithm to be $\lambda_{ii} = \lambda_{ie} = 15$. With our parameters $\nu_0^{i/i} = 4.31 \times 10^3$ s^{-1}. The full shape of D is given in Fig. 13. This is used in the numerical integrations of the Fokker–Planck equations.

We now solve the one-dimensional and two-dimensional Fokker–Planck equations, (77) and (72), numerically. At $t = 0$ both f and F are taken to be Maxwellians with temperature, T_i. The diffusion coefficient is turned on with a linear ramp function between $t = 0$ and $t = (\nu_0^{i/i})^{-1}$ and is kept constant thereafter.

Figure 14 shows the steady-state distributions. [In plotting the perpendicular distribution function in the two-dimensional case we have defined

$$F(v_\perp) = \int dv_\parallel\, f(v_\perp, v_\parallel). \tag{81}$$

Note that this is consistent with (73).] Although the dependence of f on $v_\parallel$ is not that of a Maxwellian, the two results for $F(v_\perp)$ are in close agreement. The major difference is that the tail of the distribution function is characterized by a temperature of T_i in the one-dimensional case, but by about $1.16\,T_i$ in the two-dimensional case.

The power dissipated by the wave is defined by

$$P_d = -2\pi n_0 m_i \int v_\perp^2 D\, \partial F/\partial v_\perp\, dv_\perp, \tag{82}$$

while the power lost by the test distribution to the background distributions is

$$P_c = n_0 m_i \int \sum_\beta \mathbf{v}\dot{\mathbf{J}}^{i/\beta}\, d\mathbf{v} \tag{83}$$

in the two-dimensional case and

$$P_c = 2\pi n_0 m_i \int v_\perp^2 C[\,\partial F/\partial v_\perp + (v_\perp/v_{ti}^2)F\,]\, dv_\perp \tag{84}$$

in the one-dimensional case. These are plotted as a function of time in Fig. 15. The most important quantity we wish to know is the steady-state power dissipation, P. As $t \to \infty$, we have $P = P_d = P_c$. We see that there is close agreement between the one-dimensional and two-dimensional values for P. (They differ by about 3%.) However, the solution to the one-dimensional equation reaches a steady state about 2 times faster than that of the two-dimensional equation. From Fig. 15(a) we see that P_d nearly reaches its steady-state value at $t = \tau_d \approx 6/\nu_0^{i/i} \approx 1.4$ ms, whereas P_c (and f also) reaches a steady state on a time scale, τ_c, which is about $60/\nu_0^{i/i}$ or 14 ms.

The agreement between the one- and two-dimensional treatments in the power dissipated is much better than observed in the case of the parallel one-dimensional Fokker–Planck equation for the electrons.[21] This is so because the pitch-angle scattering terms, which are the principle reason that f deviates from the form assumed in (73) are approximately 4 times less important in the case considered here. Two effects contribute to this factor of 4: In our case electrons do not cause appreciable pitch-angle scattering; whereas, in the other case, ions and electrons contribute equally. The other effect is geometrical in origin and arises because the perpendicular plane has two degrees of freedom, as opposed to the parallel direction, which has only one.

We conclude that the one-dimensional Fokker–Planck equation, (77), gives accurate results for the steady state distribution and for the power dissipated in the steady state, P. The agreement on the time scales is worse, although we expect the one-dimensional equations to give qualitatively correct results here.

XII.   ANALYTIC SOLUTION OF THE ONE-DIMENSIONAL EQUATION

We now discuss the analytical solution of the one-dimensional Fokker–Planck equation, (77). We shall be mostly concerned with the steady-state solution, since this is of the most practical interest, and accurately approximates that given by (72). We will briefly consider the time scales given by (77). The methods we use and results we obtain are very similar to those of Fisch,[19,20] who treats the parallel one-dimensional Fokker–Planck equation. Most of the analysis will be carried out for general collision term, C. We will however sometimes need to know the functional dependence of C on $v_\perp$. We shall therefore give the form of

C in the limit $v_{ti} \ll v_\perp \ll v_{te}$. Using the forms for $\nu_\perp^{\alpha/\beta}$ and $\nu_\parallel^{\alpha/\beta}$ given in Ref. 18 and assuming that $T_e = T_i$, which is required in the derivation of (77), and $\lambda_{ie} = \lambda_{ii}$ we have

$$C = \nu_0^{i/i} v_{ti}^2 \frac{3}{2} \left(\frac{v_{ti}^3}{v_\perp^3} + \frac{v_{ti}^3}{v_0^3} \right),$$
(85)

where $\nu_0^{i/i}$ is given by (80) and

$$\frac{v_0^3}{v_{ti}^3} = \frac{9Z_i}{2(2/\pi)^{1/2}} \left(\frac{m_i}{m_e} \right)^{1/2},$$
(86a)

or

$$\frac{v_0}{v_{ti}} = \begin{cases} 6.23, & \text{for hydrogen,} \\ 6.99, & \text{for deuterium,} \\ 7.48, & \text{for tritium.} \end{cases}$$
(86b)

The contributions of C_i and C_e to C are given by the first and second terms in parentheses in (85).

The steady-state solution to (77) is[20]

$$F(t \to \infty) = F_0 \exp - \int_0^{v_\perp} \frac{v_\perp/v_{ti}^2}{1 + D/C} \, dv_\perp,$$
(87a)

where F_0 is a normalization constant determined by

$$\int 2\pi v_\perp F \, dv_\perp = 1.$$
(87b)

If D is only non-zero for $v_\perp^2 \gg v_{ti}^2$ then

$$F_0 \approx (2\pi v_{ti}^2)^{-1}.$$
(88)

The power dissipated in the steady state is given by (82),

$$P = \frac{2\pi n_0 m_i}{v_{ti}^2} \int \frac{D v_\perp^3}{1 + D/C} F \, dv_\perp.$$
(89)

This power dissipation is divided between the electron and ion backgrounds according to

$$P_\beta = \frac{2\pi n_0 m_i}{v_{ti}^2} \int \frac{C_\beta D v_\perp^3}{C + D} F \, dv_\perp,$$
(90)

where P_β is the power deposited in the background species, β.

Equation (89) may be evaluated in two limits. Firstly, in the collision dominated regime, for which $D \ll C$ for all $v_\perp$, F is approximately a Maxwellian and (89) becomes

$$P = \frac{n_0 m_i}{v_{ti}^4} \int D v_\perp^3 \exp \left(-\frac{v_\perp^2}{2v_{ti}^2} \right) dv_\perp.$$
(91)

If $D(v_\perp) = 0$ for $v_\perp < v_1$ and $D(v_\perp) \approx D_0$ (a constant) for $v_1 \leq v_\perp \lesssim v_1 + v_{ti}^2/v_1$, the integral may be approximated by Laplace's method to give

$$P \approx n_0 m_i (v_1/v_{ti})^2 D_0 \exp(-\tfrac{1}{2} v_1^2/v_{ti}^2).$$
(92)

If $v_1^3 \ll v_0^3$, nearly all of this goes to ion heating.

The second limit we shall consider is the "plateau" limit, in which a plateau forms on F. Suppose $D = 0$ for $v_\perp < v_1$ or $v_\perp > v_2$ (with $v_2 > v_1$) and $D \gg C$ otherwise. If D also satisfies

$$\int_{v_1}^{v_2} \frac{Cv_\perp}{Dv_{ti}^2}\, dv_\perp \ll 1, \tag{93}$$

then F is approximately constant between v_1 and v_2. Assuming $v_1^2 \gg v_{ti}^2$, so that F_0 is given by (88), (89) becomes

$$P = \frac{n_0 m_i}{v_{ti}^4} \exp\left(-\frac{v_1^2}{2v_{ti}^2}\right) \int_{v_1}^{v_2} Cv_\perp^3\, dv_\perp. \tag{94}$$

Substituting for C from (85) we have

$$P = \tfrac{3}{2} n_0 m_i \nu_0^{i/i} v_{ti}[(v_2 - v_1) + \tfrac{1}{4}(v_2^4 - v_1^4)/v_0^3]\exp(-\tfrac{1}{2}v_1^2/v_{ti}^2), \tag{95}$$

where the first and second terms in brackets are the contributions of P to the ion and electron heating respectively.

The time scales may be readily computed for this case. Since the time scales derived from the one-dimensional equation are not very accurate, we shall merely quote the results. The derivation closely follows that given in Ref. 19. The time for the distribution to flatten between v_1 and v_2 due to D is

$$\tau_d = (v_2 - v_1)^2/D. \tag{96}$$

If $v_1(v_2 - v_1) \gg v_{ti}^2$, the time scale for particles to collisionally fill in the plateau is

$$\tau_c = \tfrac{1}{2}(v_2^2 - v_1^2)v_{ti}^2/[v_1^2\, C(v_1)], \tag{97}$$

or substituting for C, (85), with $v_1^3 \ll v_0^3$

$$\tau_c = \tfrac{1}{3}(v_2^2 - v_1^2)v_1/(v_{ti}^3 \nu_0^{i/i}). \tag{98}$$

The time scale for the saturation of P_c is τ_c, while τ_d is the time at which P_d nearly reaches its steady-state value. For $t > \tau_d$ the power required for the wave to accelerate the ions into the plateau decreases, while the power to maintain them there increases. Thus, P_d is roughly constant for $t > \tau_d$.

Many cases of interest will not be in the collisional or plateau limits. However, we may still obtain approximate results by judiciously taking one or other limit. For instance, if we consider the case treated in the previous section, we see that a plateau has formed over part of the range where D is finite, Fig. 14(b). The plateau limit has some validity in this case since D cuts off quite sharply at the low velocity end, Fig. 13, and so the height of the plateau is fairly well determined. We take v_1 to be given by

$$D(v_1) = C(v_1) \tag{99a}$$

and v_2 by

$$\int_{\omega/k_\perp}^{v_2} \frac{Cv_\perp}{Dv_{ti}^2}\, dv_\perp = 1. \tag{99b}$$

(Thus, at v_2, F is a factor, e, lower than the plateau height.) These give $v_1 = 3.1\, v_{ti}$ and $v_2 = 5.9\, v_{ti}$, approximately. We then obtain

$$P \approx 5 \times 10^{-2}\, n_0 m_i v_{ti}^2 \nu_0^{i/i}. \tag{100}$$

About 70% of this goes to heating the ions. Equation (100) is fairly close to the observed value for which the numerial factor is 3.8×10^{-2}, Fig. 15(a). By far the most sensitive factor in determing P is v_1, since the height of the plateau depends exponentially on v_1. More accurate estimates of the plateau height are possible. However, if a more accurate result that (100) is required, it is probably easiest just to evaluate (87) and (89) numerically.

With these values of v_1 and v_2 the time scale become $\tau_d = 5/\nu_0^{i/i}$ [taking D to be given by (79)] and $\tau_c = 26/\nu_0^{i/i}$. These agree quite well with the results of the numerical solution of (77) given in Fig. 15(b). However, as we noted these times (and, in particular, τ_c) differ from the times given by the two-dimensional Fokker–Planck equation.

XIII.   DISCUSSION

We have computed the rate of diffusion of ions in perpendicular velocity space in the presence of a uniform magnetic field and a perpendicularly propagating electrostatic wave for which $\omega \gg \Omega_i$. The diffusion coefficient is given by (69). From the results of I, it is seen that this diffusion coefficient also applies to diffusion in a lower hybrid wave (for which $k_\parallel$ is finite, but $k_\parallel \ll k_\perp$) in a weakly inhomogeneous magnetic field. The effect of nonuniformity of the lower hybrid wave is modeled by introducing the geometrical factor, γ, into (69).

In order to determine the heating rate, collisions are included, and a one-dimensional Fokker–Planck equation, (77), is derived. From this the steady-state power dissipation, P, may be found, (89). Provided $\omega/(k_\perp v_{ti})$ becomes sufficiently small (on the order of 4) this may result in strong damping of the lower hybrid wave and efficient heating of the ions. (See the example in Sec. XI.)

These results may be used in a simulation of lower hybrid heating with a transport code, provided the time scale for the evolution of the plasma exceeds τ_c. The quantities, P_e and P_i, (90), which represent the powers deposited per unit volume, would then appear as source terms in the equations for the electrons and ions. The wave would obey an evolution equation

$$v_{gr}\, \partial W(r,t)/\partial r = -P(r,t)/\gamma, \tag{101}$$

where W is the energy density of the wave, r is the minor radius of the tokamak, and v_{gr} is the radial group velocity. In this equation t is a parameter. P and W would vary with time as the background distributions evolve.

Lastly we consider the question of particle transport due to stochastic heating. Firstly, there is the change in the transport coefficients due to the altered distribution function of the ions, Fig. 14. Since the heating initially takes place in the perpendicular direction, this would lead to an increase in the number of trapped ions, which may have a deleterious effect on the transport. Secondly, the equations of motion, (2), give a shift in the guiding centers of the ions. The amount of this shift is most easily calculated from the Hamiltonian, (A1), since $-I_2$ is the x guiding center position. (There is no shift in the y guiding center.) Thus, we have $-\Delta I_2 = \Delta I_1/\nu$ (after averaging over a cyclotron period) or, undoing the normalizations

$$\Delta \mathbf{x} = (k_\perp/\omega)\, \Delta\mu\, \hat{\mathbf{k}} \times \hat{\mathbf{B}}, \tag{102}$$

where μ is the magnetic moment, $\frac{1}{2}m_i v_\perp^2/(q_i B_0)$. When considering heating by the injected lower hybrid wave (rather than parametric decay products) $\mathbf{k}$ is mainly in the radial direction and so $\Delta \mathbf{x}$ is mostly in the poloidal direction. So this effect does not lead to any outward transport of ions.

ACKNOWLEDGMENTS

APPENDIX A: DIFFERENCE EQUATIONS FROM THE HAMILTONIAN

In this appendix we derive the difference equations, (13), from the Hamiltonian for the ion. Using this approach it is easy to establish what approximations are made. In I it was shown that the motion of an ion in the fields, (1), is governed by the Hamiltonian,

$$H = I_1 + \nu I_2 - \alpha \sin[(2I_1)^{1/2} \sin w_1 - w_2]$$

$$= I_1 + \nu I_2 - \alpha \sum_{m=-\infty}^{\infty} J_m[(2I_1)^{1/2}] \sin(mw_1 - w_2), \tag{A1}$$

where the normalizations are the same as used in (2), J_m is the Bessel function of order m, $y = (2I_1)^{1/2} \sin w_1$, and $x = -I_2 - (2I_1)^{1/2} \cos w_1$. The action variable, I_1, is related to the Larmor radius, r (3c), by $I_1 = \frac{1}{2} r^2$. We now perform a series of transformations, similar to those made in Appendix C of I, to bring the sum in (A1) into the form of an infinite sum of the product of two trigonometric terms. Hamilton's equations of motion may then be written in terms of delta functions.

We first transform (A1) to hatted variables using the generating function,

$$F_2 = \hat{I}_1(nw_1 - w_2) + \hat{I}_2 w_2, \tag{A2}$$

where n is given by (15). Equation (A1) then becomes

$$\hat{H} = -\delta \hat{I}_1 + \nu \hat{I}_2 - \alpha \sum_m J_m[(2n\hat{I}_1)^{1/2}] \sin\left[\frac{m}{n}\hat{w}_1 - \left(1 - \frac{m}{n}\right)\hat{w}_2\right]. \tag{A3}$$

Since $\hat{w}_1$ is slowly varying, whereas $\hat{w}_2$ is still rapidly varying (assuming $n \gg 1$) the dominant contributions to the sum in (A3) come from $m \approx n$. Recognizing this we replace m by $n+k$ in the sum to obtain

$$\hat{H} = -\delta \hat{I}_1 + \nu \hat{I}_2 - \alpha \sum_{k=-N}^{N} J_{n+k}[(2n\hat{I}_1)^{1/2}] \sin\left[\left(1 + \frac{k}{n}\right)\hat{w}_1 + \frac{k}{n}\hat{w}_2\right], \tag{A4}$$

where N is some integer satisfying $1 \ll N \ll n$. [It is convenient to choose $N \approx (\frac{1}{2}\nu)^{1/3}$.] As a result of this inequality we approximate the factor $(1 + k/n)$ by unity. We next use the large argument expansion of the Bessel function

$$J_m(r) = (2/\pi)^{1/2}(r^2 - m^2)^{-1/4}$$

$$\times \cos[(r^2 - m^2)^{1/2} - m\cos^{-1}(m/r) - \pi/4] \tag{A5}$$

[Ref. 3, Eq. (9.3.3)], which is valid for $r > m + (\frac{1}{2}m)^{1/3}$. In order to put the Hamiltonian into the required form we need to be able to do three things: approximate all the Bessel

functions in (A4) using (A5), which requires $r > (n + N) + (\frac{1}{2}n)^{1/3}$; replace the amplitude factor $(r^2 - m^2)^{-1/4}$ by $(r^2 - \nu^2)^{-1/4}$, which requires $r^2 - n^2 \gg Nn$; and to Taylor-expand the argument of the cosine in (A5) in k about $k = \delta$, keeping only the first two terms, which requires $r^2 - n^2 \gg N^4$. With $N \approx (\frac{1}{2}\nu)^{1/3}$ all these inequalities become $r - \nu \gg (\frac{1}{2}\nu)^{1/3}$. The Bessel functions in (A4) then become

$$J_{n+k}(r) = (2/\pi)^{1/2}(r^2 - \nu^2)^{-1/4} \cos(R - k\phi + \delta\phi), \tag{A6}$$

where $r = (2n\hat{I}_1)^{1/2}$, $R = g(r) \equiv (r^2 - \nu^2)^{1/2} - \cos^{-1}(\nu/r) - \pi/4$, and $\phi = \cos^{-1}(\nu/r)$. We shall regard the r's appearing in the amplitude factor and in the definition of ϕ as being parameters. This requires that neither of these quantities change significantly when r changes by a period of the Bessel function, $2\pi(\partial R/\partial r)^{-1}$. The conditions on r and ν already assumed are sufficient to guarantee this. In addition, if α exceeds the stochasticity threshold, r may change by more than the period of the Bessel function, in which case we must re-examine our assumptions about the constancy of the amplitude factor and ϕ. We shall return to this point after we have derived the difference equations.

We now transform to a new set of variables, distinguished by tildes, using the generating function,

$$F_3 = -G(\hat{I}_1)\tilde{w}_1 - \hat{I}_2\tilde{w}_2, \tag{A7}$$

where $G(\hat{I}_1) \equiv g[(2n\hat{I}_1)^{1/2}]$. This gives

$$\tilde{I}_1 = G(\hat{I}_1), \qquad \hat{w}_1 = G'(\hat{I}_1)\tilde{w}_1. \tag{A8}$$

We solve both of these locally by expanding $\hat{I}_1$ about some point $\hat{I}_{10}$ and keeping only the terms involving $G'(\hat{I}_{10})$. Thus, we obtain

$$\hat{I}_1 = \tilde{I}_1/G'(\hat{I}_{10}) + \text{const.}, \qquad \hat{w}_1 = G'(\hat{I}_{10})\tilde{w}_1. \tag{A9}$$

This is consistent with the approximations already made. Writing $G'(\hat{I}_{10})$ in terms of the Larmor radius, r (which, like $\hat{I}_{10}$, we regard as constant), we have

$$G'(\hat{I}_{10}) = g'(r)\,\partial r/\partial\hat{I}_1 \approx (r^2 - \nu^2)^{1/2}\nu/r^2 \equiv Q. \tag{A10}$$

The Hamiltonian becomes

$$\tilde{H} = -\frac{\delta}{Q}\tilde{I}_1 + \nu\tilde{I}_2$$
$$- \frac{\alpha(2/\pi)^{1/2}}{(r^2 - \nu^2)^{1/4}} \sum_k \cos(\tilde{I}_1 - k\phi + \delta\phi)\sin\left(Q\tilde{w}_1 + \frac{k}{n}\tilde{w}_2\right). \tag{A11}$$

Finally, we perform the scaling transformation,

$$M = Q\tilde{H}, \tag{A12a}$$

$$J_1 = \tilde{I}_1, \qquad \psi_1 = Q\tilde{w}_1, \tag{A12b}$$

$$J_2 = Q\nu\tilde{I}_2, \qquad \psi_2 = \tilde{w}_2/\nu, \tag{A12c}$$

so that the Hamiltonian is given by

$$M = -\delta J_1 + J_2 - A \sum_{k=-\infty}^{\infty} \cos(J_1 - k\phi + \delta\phi)\sin(\psi_1 + k\psi_2), \tag{A13}$$

where A is given by (11) and we have approximated ν/n by unity to give the last term in the argument to the sine. We have extended the limits of the sum to infinity; the additional terms introduced are non-resonant, and so do not have much effect.

Hamiltons's equations now give $\dot{\psi}_2 = 1$ or $\psi_2 = t$ and

$$\dot{\psi}_1 = -\delta + A \sum_k \sin(J_1 - k\phi + \delta\phi) \sin(\psi_1 + kt), \tag{A14a}$$

$$\dot{J}_1 = A \sum_k \cos(J_1 - k\phi + \delta\phi) \cos(\psi_1 + kt). \tag{A14b}$$

Defining new variables,

$$\gamma = n\pi - \psi_1, \qquad \rho = J_1 + \nu\pi, \tag{A15a}$$

$$u = \gamma - \rho, \qquad v = \gamma + \rho, \tag{A15b}$$

we find

$$\dot{u} = \delta - A \sum_k \cos[v - (\pi - \phi)\delta - k(t + \phi)]$$

$$= \delta - 2\pi A \cos[v - (\pi - \phi)\delta] \sum_{j=-\infty}^{\infty} \hat{\delta}(t + \phi - 2\pi j), \tag{A16a}$$

$$\dot{v} = \delta + A \sum_k \cos[-u - (\pi - \phi)\delta + k(t - \phi)]$$

$$= \delta + 2\pi A \cos[u + (\pi - \phi)\delta] \sum_{j=-\infty}^{\infty} \hat{\delta}(t - \phi - 2\pi j). \tag{A16b}$$

We have used the notation, $\hat{\delta}$, to denote the Dirac delta function (to distinguish it from the variable, δ) and we have used the identity,

$$\sum_{k=-\infty}^{\infty} \cos kt = 2\pi \sum_{j=-\infty}^{\infty} \hat{\delta}(t - 2\pi j). \tag{A17}$$

Defining $u_j = u(t = 2\pi j - \pi)$ and similarly for v, we may obtain

$$u_{j+1} - u_j = 2\pi\delta - 2\pi A \cos v_j, \tag{A18a}$$

$$v_{j+1} - v_j = 2\pi\delta + 2\pi A \cos u_{j+1}. \tag{A18b}$$

It is readily established that ρ as given by (A15a) agrees with (6a), and that γ at $\psi_2 = 2\pi j - \pi$ is equal to w_2 at $w_1 = 2\pi j - \pi$ and so is equal to θ_j as defined in (6b). Thus, the difference equations given in (A18) agree with those derived in Sec. II, (13). The final condition on the validity of (A18) is that the change in ρ in one iteration is insufficient to cause an appreciable change in A through r. (This then justifies taking A to be a constant.) The maximum change in ρ in one iteration is on the order of A. Therefore the fractional change in A due to this change in ρ is

$$A \frac{\partial \log A}{\partial \rho} = \frac{\partial A}{\partial \rho} = \frac{\partial A}{\partial r} \frac{\partial r}{\partial \rho} \sim \frac{\alpha\nu}{(r^2 - \nu^2)^{5/4}}, \tag{A19}$$

where, in differentiating A we have only considered its dependence on r through $(r^2 - \nu^2)^{1/4}$. Demanding that (A19) be small gives

$$\alpha \ll (r^2 - \nu^2)^{5/2}/\nu \quad \text{or} \quad A \ll (r^2 - \nu^2)^{3/2}/r^2. \tag{A20}$$

The other assumptions made are $\nu \gg 1$ and $r - \nu \gg (\frac{1}{2}\nu)^{1/3}$.

APPENDIX B: FIRST-ORDER ACCELERATOR MODES

We consider here the simplest of the accelerator modes. Such modes are island systems around first-order fixed points in the (u, v) plane; i.e., points for which $u_1 - u_0 = -2\pi n$ and $v_1 - v_0 = 2\pi m$, where m and n are integers. The amount by which ρ increases per iteration is $s\pi$, where $s = m + n$. From (13) the fixed points are given by

$$\delta + A \cos u_0 = m, \qquad \delta - A \cos v_0 = -n. \tag{B1}$$

In order for an island to exist, the fixed point, (u_0, v_0), must be elliptic. The stability of (u_0, v_0) is determined by the eigenvalues of the linearized mapping. From (35) we have

$$\mathbf{J}_0 = \begin{pmatrix} 1 & 2V \\ -2U & 1 - 4UV \end{pmatrix}, \tag{B2}$$

where $U = \pi A \sin u_0$ and $V = \pi A \sin v_0$. The eigenvalues are given by

$$\lambda = 1 - 2UV \pm 2(U^2 V^2 - UV)^{1/2}. \tag{B3}$$

The fixed point is elliptic if λ is complex, which requires $0 < UV < 1$. Substituting for $\sin u_0$ and $\sin v_0$ gives

$$A^2 - (m - \delta)^2 > 0, \tag{B4a}$$

$$A^2 - (n + \delta)^2 > 0, \tag{B4b}$$

$$[A^2 - (m - \delta)^2][A^2 - (n + \delta)^2] < 1/\pi^4, \tag{B4c}$$

as the conditions for first-order accelerator modes. When $|A|$ just exceeds $\max(|m - \delta|,$ $|n + \delta|)$ then (B4) is satisfied. At this point elliptic and hyperbolic fixed points appear (with different signs for $\cos u_0$ or $\cos v_0$). As $|A|$ is increased further (B4c) fails and the elliptic fixed point turns into a hyperbolic fixed point with reflection. Thus, (B4) defines a range, $A_\ell < |A| < A_u$, which is a function of δ, m, and n, in which first-order elliptic fixed points exist.

Figure 16 shows the behavior of the mode with $m = 1$ and $n = 0$ for $\delta = \frac{1}{2}$. From (B4) we see that for these parameters $A_\ell = \frac{1}{2}$ and $A_u = (\frac{1}{4} + \pi^{-2})^{1/2} = 0.5927$. At $A = 0.55$, Fig. 16(a), the first-order island is visible. This is surrounded by higher-order (4th and 32nd) accelerator modes. When A just exceeds A_u, Fig. 16(b), the center of the first-order island becomes unstable, becoming a hyperbolic fixed point, separating two second-order islands. However, although this point is unstable, it is confined to the island system, since there are still eigencurves with the original topology surrounding the system of two islands and one hyperbolic fixed point. Thus, a point started close to the hyperbolic point will be forever accelerated. These eigencurves are soon destroyed, however, allowing the escape of particles starting near the fixed point. In Fig. 16(c) we see that the particle spends on the order of 1000 iterations encircling the second-order islands before escaping. As A is

increased further, the second-order islands rapidly decrease in size, becoming unstable when A is slightly greater that 0.601.

From Fig. 16 we see that we should study accelerator modes of many different orders in order to have a complete understanding of their effect on the diffusion of particles. However, while it is possible to thoroughly study first-order fixed points, just cataloguing the higher-order fixed points becomes a monumental task for $A \gtrsim 1$. For example, there are over 100 second-order fixed points present for $A = 1$. We will therefore pursue only the first-order fixed points.

In Fig. 17 we show the range in $|A|$ defined by (B4) as a function of δ with $s = 0$, 1, and 2. (For each value of s, all values of m and n satisfying $m + n = s$ are considered.) The pattern evident in these figures is repeated for higher values of s. From (B4) and Fig. 17 we see that an accelerator mode, with a given value of s, first appears at

$$A_\ell = \begin{cases} |s/2| + |\delta|, & \text{for } s \text{ even,} \\ |s/2| + \frac{1}{2} - |\delta|, & \text{for } s \text{ odd.} \end{cases} \tag{B5}$$

(Recall that δ is defined such that $|\delta| \leq \frac{1}{2}$.)

The accelerator mode disappears at a slightly higher amplitude, but periodically reappears (with different m and n, but the same s) at

$$A_\ell = \begin{cases} |s/2| \pm |\delta| + p, & \text{for } s \text{ even,} \\ |s/2| \pm (\frac{1}{2} - |\delta|) + p, & \text{for } s \text{ odd,} \end{cases} \tag{B6}$$

where p is a positive integer. For a given s, the gap in which the accelerator mode exists, $\Delta A \equiv A_u - A_\ell$, is widest when $A_\ell = |s/2|$, $\delta = 0$ for s even and $|\delta| = \frac{1}{2}$ for s odd. In this case we have

$$A_u = \left(\frac{s^2}{4} + \frac{1}{\pi^2} \right)^{1/2}. \tag{B7}$$

For $s = 0$ (i.e., no acceleration), we have $A_\ell = 0$ and $A_u = 1/\pi$. This is the range in which the central fixed points of the islands in Fig. 3(a) are stable. If $|s| \gg 1$ then

$$\Delta A = \frac{1}{2\pi^2 A_\ell}. \tag{B8}$$

When $|A|$ greatly exceeds the minimum threshold for a given s, so the A_ℓ is given by (B6) with $p \gg 1$, we may find an approximate solution for ΔA from (B4):

$$\Delta A = \begin{cases} \dfrac{1}{2\pi^2 A_\ell}, & \text{for } s = 0, \\[2mm] \dfrac{1}{4\pi^4 s A_\ell^2}, & \text{for } s \neq 0. \end{cases} \tag{B9}$$

Since the number of first-order accelerator modes increases with increasing A (see Fig. 17), we are lead to ask how the fraction of phase space occupied by accelerator modes varies with increasing A. We try to find an upper bound on this quantity for the first-order modes. We estimate the size of an accelerator mode by noting that the maximum radius of the island is given by the distance between the elliptic and hyperbolic fixed points. We consider here the pair of fixed points that are born together and we assume that the islands are roughly circular. From (B1) this distance is about $[(A - A_\ell)/A_\ell]^{1/2}$ (ignoring numerical factors). This is maximaized by letting $A = A_u$. The maximum area of the island is then $\Delta A/A_\ell$.

For a given A, modes with s from 1 to about $2A$ can be present; thus, the total area of the accelerator modes is on the order of

$$\sum_{s=1}^{2A} \frac{\Delta A}{A_\ell} \sim \sum_{s=1}^{2A} \frac{1}{sA^3} \sim \frac{\log A}{A^3}. \tag{B10}$$

Here we have used the form of ΔA for $p \gg 1$ and $s \neq 0$, (B9). If $\delta = 0$ or $\frac{1}{2}$ then there is an additional contribution of order A^{-2} from the mode that just appeared for the first time by satisfying (B5); in this case ΔA is given by (B8). This then dominates over (B10). In either case the area of the accelerator modes decreases with A.

However, the modes tend to line up close to $\cos u = 0$ and $\cos v = 0$, since (B4a), say, may be well satisfied, when (B4b) becomes true. We should investigate whether the modes can form a barrier inhibiting the diffusion of particles. The sum of the widths of the accelerator modes is

$$\sum_{s=1}^{2A} (sA^3)^{-1/2} \sim A^{-1}, \tag{B11}$$

which also decreases with A.

We conclude that the effect of the first-order accelerator modes decreases with increasing A. This leaves open the possibility that the effect of all the accelerator modes may not decrease. We have, however, observed no evidence of this.

APPENDIX C: MONTE CARLO SOLUTION

We describe here the solution of (66) by a Monte Carlo method. We first define a new velocity coordinate, $\mu = \frac{1}{2} r^2$, so that (66) becomes

$$\frac{\partial f}{\partial t} = \frac{\partial}{\partial \mu} r^2 D \frac{\partial}{\partial \mu} f. \tag{C1}$$

(The variable μ is proportional to the magnetic moment and is the same as the action, I_1, used in Appendix A.) We solve (C1) by dividing each cyclotron period up into M equal time intervals of $2\pi/M$. The distribution function is recorded by the positions of N particles, $\mu_{i,j}$, where the subscript, i, refers to the particle number and j to the time step, $j = Mt/2\pi$. The distribution function, f, is found by converting μ back to r and letting

$$f(r) = \frac{\delta N}{2\pi N r \, \delta r}, \tag{C2}$$

where δN is the number of particles with velocity between $r - \delta r/2$ and $r + \delta r/2$. We advance f by the difference equation,

$$\mu_{i,j+1} - \mu_{i,j} = \begin{cases} +\delta^+, & \text{with probability } \frac{1}{2}, \\ -\delta^-, & \text{with probability } \frac{1}{2}. \end{cases} \tag{C3}$$

[Do not confuse $\delta^\pm$ with the parameter, δ, defined in (15).] In the limit, $M \to \infty$, both δ^+ and δ^- are given by $\delta(\mu)$, where

$$\delta(\mu) \equiv (2\pi r^2 D/M)^{1/2}. \tag{C4}$$

However, there are corrections to the expressions of δ^+ and δ^- of order M^{-1} which must be included if we are to correctly model (66). [If we do not include these corrections we end up

solving the equation, $\partial f / \partial t = (\partial^2 / \partial \mu^2) r^2 D f$.] We derive these corrections by demanding that the steady-state solution given by the (C3) agrees with the steady-state solution to (C1), viz., $f = $ const. Letting f be a constant (which we take to be unity), the flux of particles, S, at μ is

$$S(\mu) = \tfrac{1}{2}[\delta^+(\mu - \epsilon^+) - \delta^-(\mu + \epsilon^-)], \tag{C5}$$

where

$$\epsilon^+ = \delta^+(\mu - \epsilon^+), \qquad \epsilon^- = \delta^-(\mu + \epsilon^-). \tag{C6}$$

Equation (C5) just expresses the fact that half the particles between $\mu - \epsilon^+$ and μ will pass the point μ is one time step, and similarly for the particles between μ and $\mu + \epsilon^-$. Setting $S(\mu)$ to zero gives

$$\delta^-(\mu + \epsilon) = \delta^+(\mu - \epsilon) = \epsilon. \tag{C7}$$

Putting $\epsilon = \delta(\mu)$ we recover the correct result for δ^+ and δ^- in the limit, $M \to \infty$. This gives

$$\delta^-[\mu + \delta(\mu)] = \delta^+[\mu - \delta(\mu)] = \delta(\mu). \tag{C8}$$

Equation (C8) has a very simple graphical representation which is shown in Fig. 18. In the limits, $M \to \infty$ and $\delta \to 0$, we can make a Taylor series expansion about μ to give

$$\delta^+(\mu) - \delta^-(\mu) = d(\delta^2)/d\mu. \tag{C9}$$

This acts as a friction force which appears in the diffusion equation, (C1), when we write it in the form,

$$\frac{\partial f}{\partial t} = -\frac{\partial}{\partial \mu}\left[\left(\frac{\partial r^2 D}{\partial \mu}\right) f - \frac{\partial}{\partial \mu}(r^2 D f)\right]. \tag{C10}$$

From Fig. 18 we see that δ^+ or δ^- becomes double-valued if $|d\delta/d\mu| > 1$. This can always be prevented by choosing M large enough. However, from the definition of D, (67), we see that D has quite large gradients for $r < \nu - \sqrt{\alpha}$. We avoid choosing M to be large to compensate for this by defining $\delta^+(\mu)$ to be $\delta(\mu)$ and basing the definition of δ^- on δ^+ with

$$\delta^-[\mu + 2\delta^+(\mu)] = \delta^+(\mu) = \delta(\mu), \tag{C11}$$

which is obtained by letting $\epsilon = \delta(\mu - \epsilon)$ in (C7). In the limit, $M \to \infty$, (C11) agrees with (C8).

To summarize: We solve (C1) and hence (66) using the difference scheme, (C3), with δ^+ and δ^- defined by (C11) and (C4). M is chosen to be 25.

References

[1] C. F. F. Karney, Phys. Fluids **21**, 1584 (1978).

[2] Y. Gell and R. Nakach, in *Plasma Physics and Controlled Nuclear Fusion Research 1978*, (International Atomic Energy Agency, Vienna), paper IAEA–CN–37–G–1 (to be published).

[3] M. Abramowitz and I. A. Stegun (editors), *Handbook of Mathematical Functions*, (U. S. Government Printing Office, Washington, D.C., 1964).

[4] C. F. F. Karney, Ph.D. thesis, Massachusetts Institute of Technology (1977).

[5] A. V. Timofeev, Nucl. Fusion **14**, 165 (1974).

[6] The Mathlab Group, *MACSYMA Reference Manual*, Version 9, Laboratory for Computer Science, Massachusetts Institute of Technology (1977).

[7] M. V. Berry, in *Topics in Nonlinear Dynamics*, edited by S. Jorna, Am. Inst. Phys. Conf. Proc., No. 46 (American Institute of Physics, 1978), p. 16.

[8] J. Ford, in *Fundamental Problems in Statistical Mechanics*, edited by E. D. G. Cohen (North-Holland, Amsterdam, 1975), Vol. 3, p. 215.

[9] B. V. Chirikov, Phys. Repts. **52**, 263 (1979).

[10] V. I. Arnold, *Mathematical Methods of Classical Mechanics*, translated by K. Vogtmann and A. Weinstein (Springer-Verlag, 1978).

[11] J. M. Greene, J. Math. Phys. **20**, 1183, (1979).

[12] A. Fukuyama, H. Momota, R. Itatani, and T. Takizuka, Phys. Rev. Lett. **38**, 701 (1977).

[13] S. Chandrasekhar, Rev. Mod. Phys. **15**, 1 (1943).

[14] M. C. Wang and G. E. Uhlenbeck, Rev. Mod. Phys. **17**, 323 (1945).

[15] E. Lazarro, Lettere al Nuovo Cimento **22**, 625 (1978).

[16] R. J. Briggs and R. R. Parker, Phys. Rev. Lett. **29**, 852 (1972).

[17] B. A. Trubnikov, in *Reviews of Plasma Physics*, edited by M. A. Leontovich (Consultants Bureau, N.Y., 1965), Vol. 1, p. 105.

[18] D. L. Book, *NRL Plasma Formulary*, Naval Research Lab. (1978).

[19] N. J. Fisch, Ph.D. thesis, Massachusetts Institute of Technology (1978).

[20] N. J. Fisch, Phys. Rev. Lett. **41**, 873 (1978).

[21] C. F. F. Karney and N. J. Fisch, Phys. Fluids **22**, 1810, (1979).
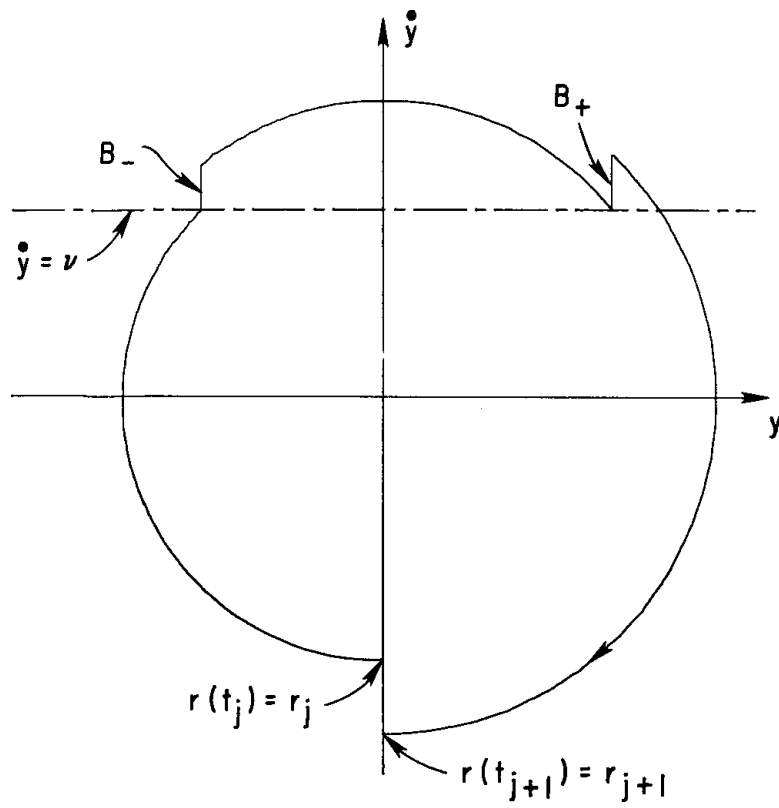
Fig. 1. Motion of an ion in velocity space, showing the kicks it receives when passing through wave-particle resonance.
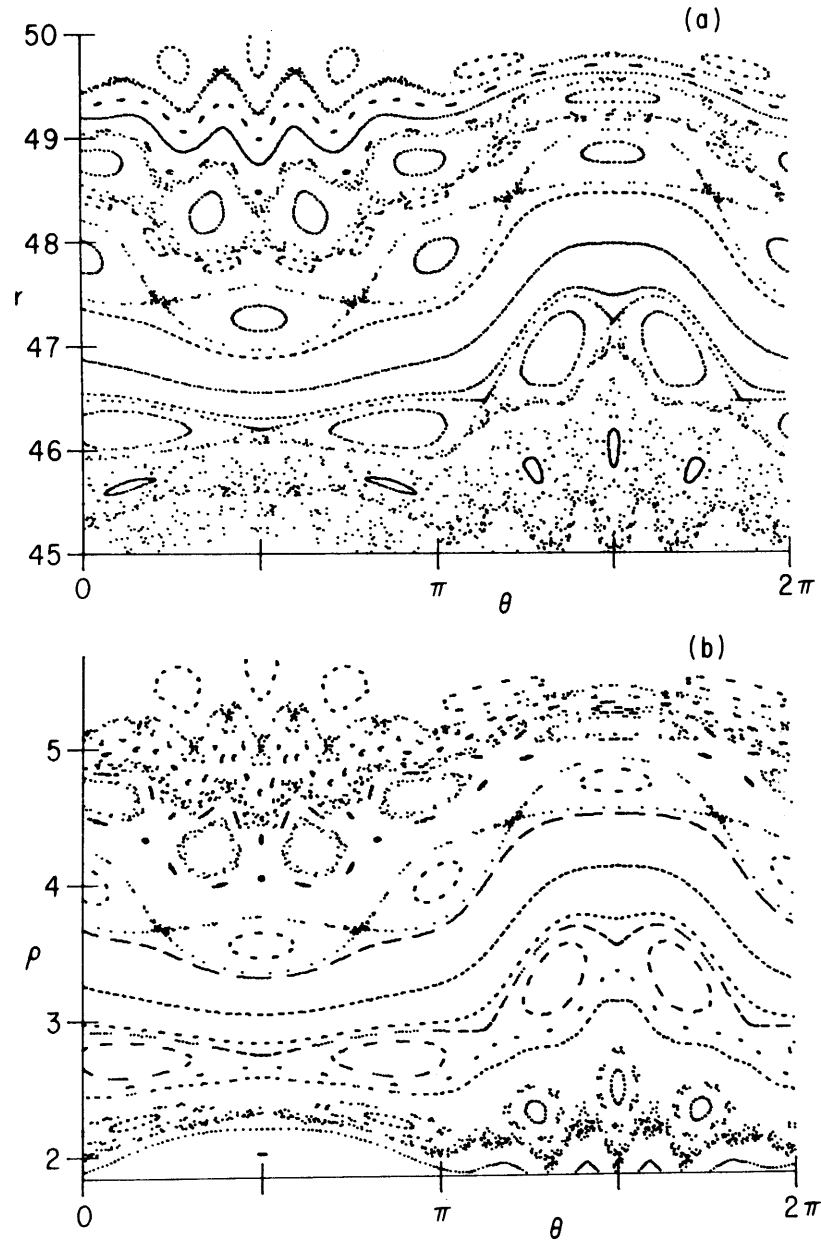
Fig. 2. Comparison of the difference equations, (13), with the Lorentz force law, (2). (a) The mapping of the (θ, r) plane using (2) with $\nu = 30.23$ and $\alpha = 2.2$. [This is taken from Fig. 3(b) of I.] (b) The mapping of the (θ, ρ) plane under T using (13), with $\delta = 0.23$ and $A = 0.1424$, which is given by (11) with $\nu = 30.23$, $\alpha = 2.2$, and $r = 47.5$. In each case the trajectories of 24 particles are followed for 300 orbits. Thus, in (b) the points, $T^j(\theta_0, \rho_0)$ for $0 \leq j \leq 300$, are plotted for 24 different initial conditions, (θ_0, ρ_0).
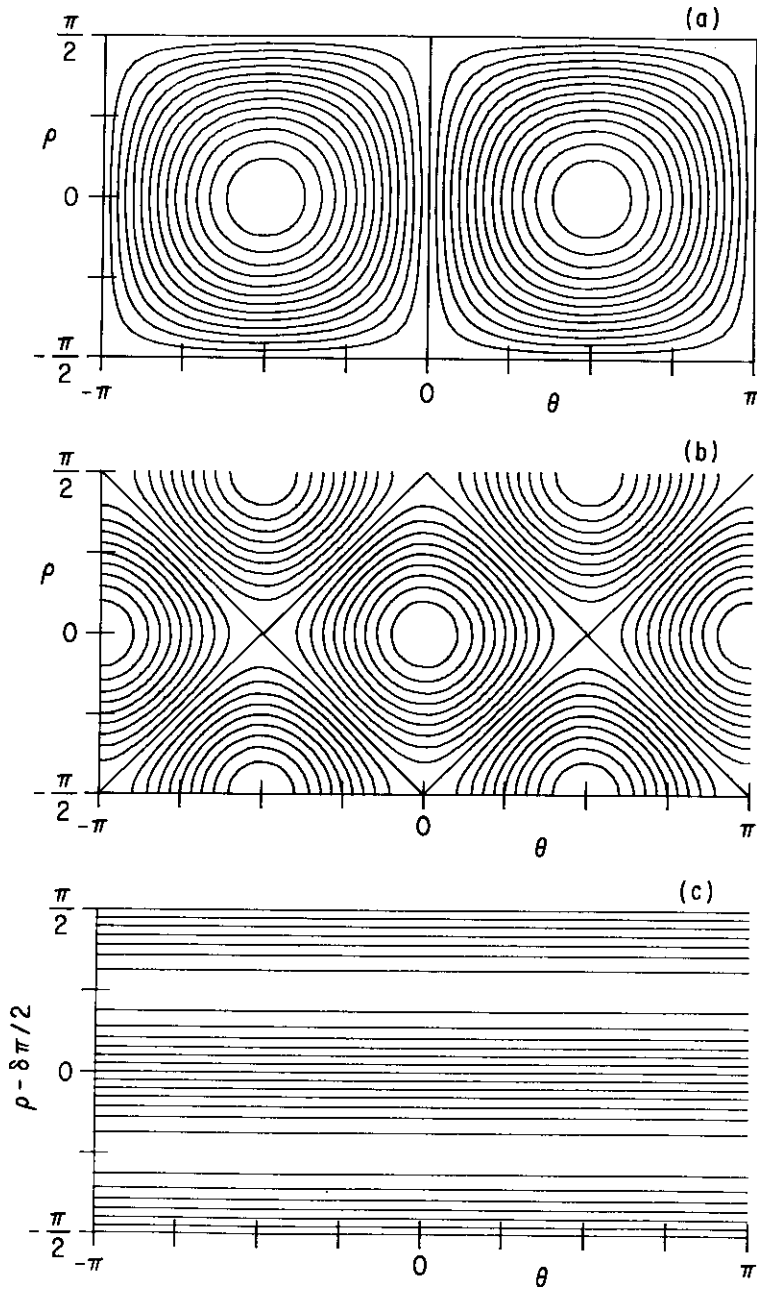
Fig. 3.   Trajectories in the (θ, ρ) plane for small A and (a) $\delta = 0$, (b) $\delta = \frac{1}{2}$, (c) $\delta = s/p$ (not equal to 0 or $\frac{1}{2}$). The trajectories are obtained by plotting curves for which the Hamiltonian, h, is constant.
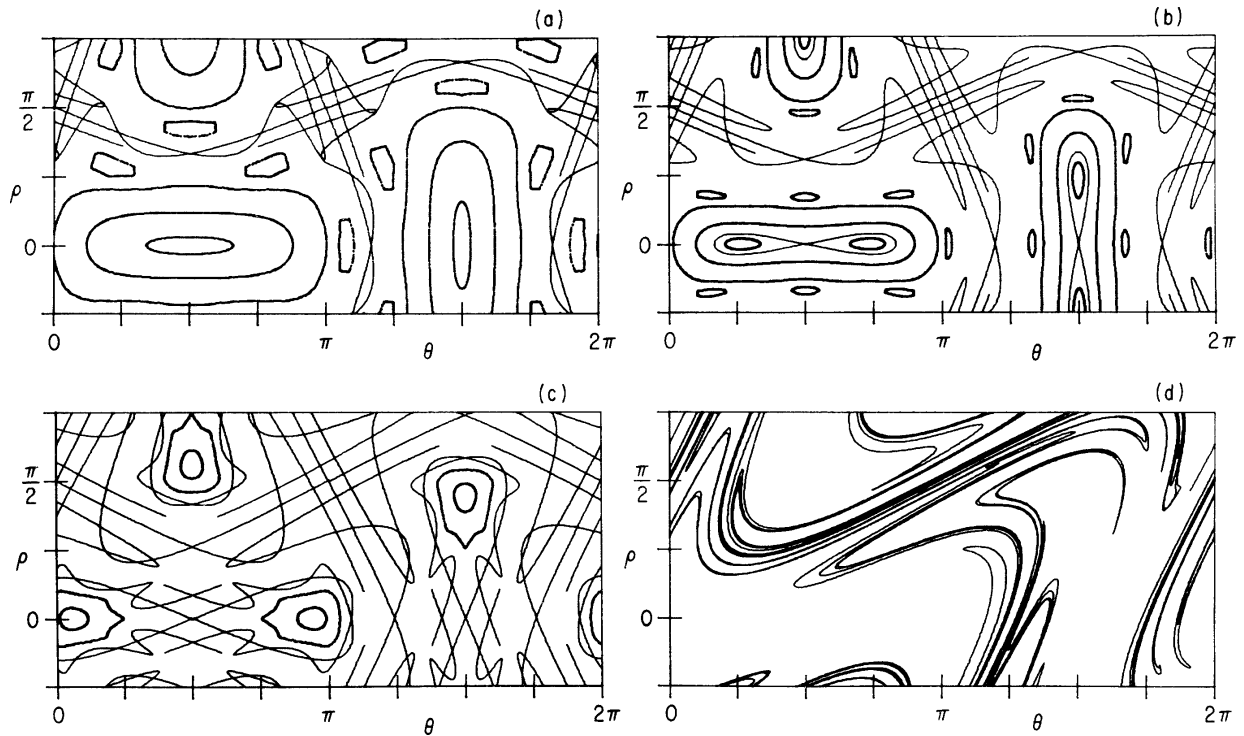
Fig. 4.   Eigencurves of the mapping, T, for $\delta = 0$ and (a) $A = 0.3$, (b) $A = 0.35$, (c) $A = 0.45$. (d) The extension of one of the eigencurves in (c) emanating from the hyperbolic fixed point with reflection.
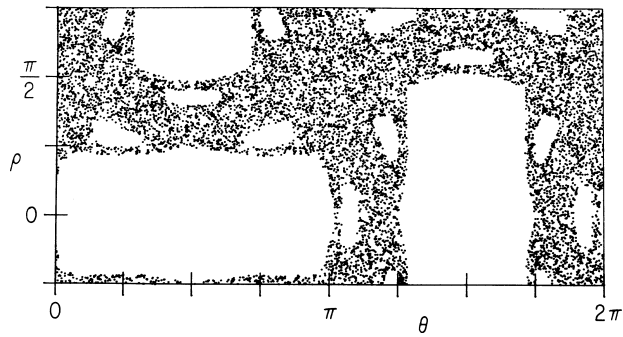
Fig. 5.   The iterates of a single point for $\delta = 0$ and $A = 0.3$. The point is chosen to start on one of the eigencurves emanating from the hyperbolic fixed point and $10\,000$ iterates are shown. Compare with Fig. 4(a).
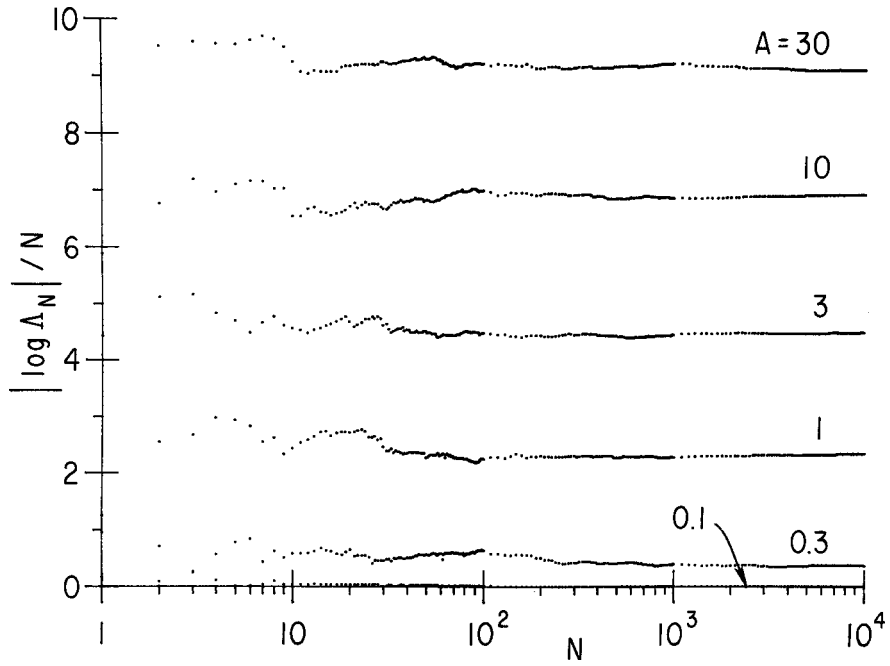
Fig. 6. Plot of $\log |\Lambda_N| /N$ as a function of N for various values of A. Here $\delta = 0.23$ and the reference trajectory was begun at $u_0 = 2$, $v_0 = 6$.
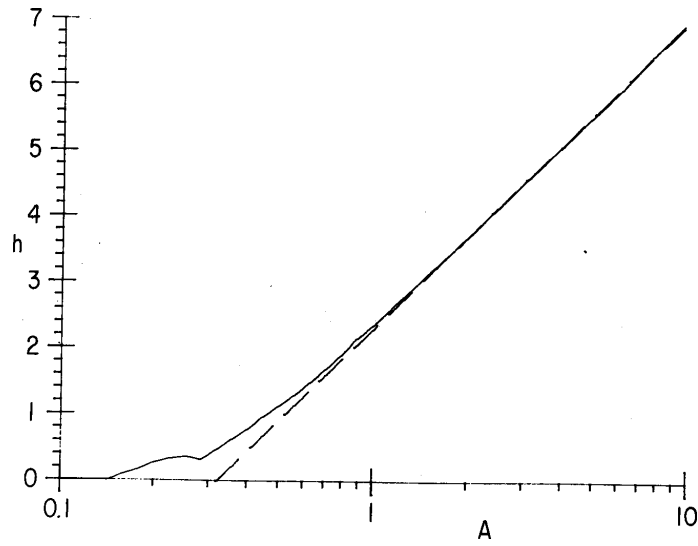
Fig. 7. Plot of h against A for $\delta = 0.23$, $u_0 = 2$, $v_0 = 6$. The dashed line is the asymptotic result, (43).
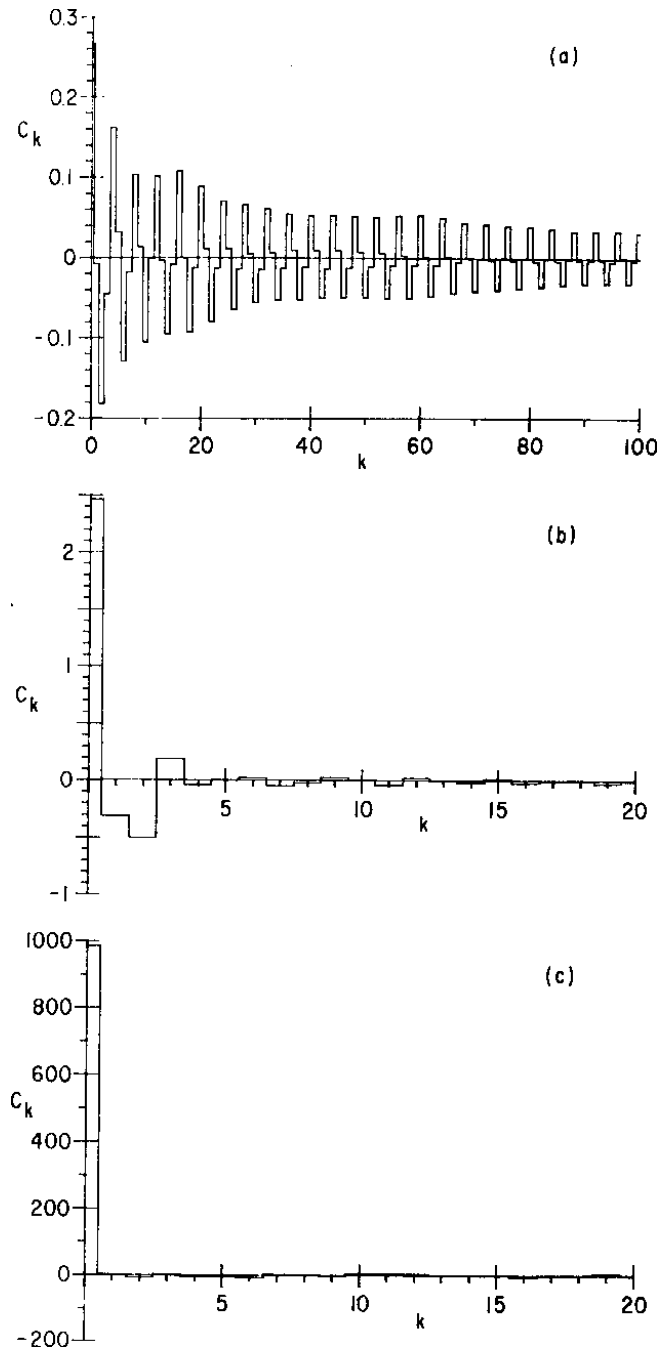
Fig. 8.   The correlation function, C_k, for $\delta = 0.23$ and (a) $A = 0.2$, (b) $A = 0.5$, (c) $A = 10$. C_k was computed using (53) with $M = 10$ and $L = 5000$. The orbits were all chosen in the stochastic region.
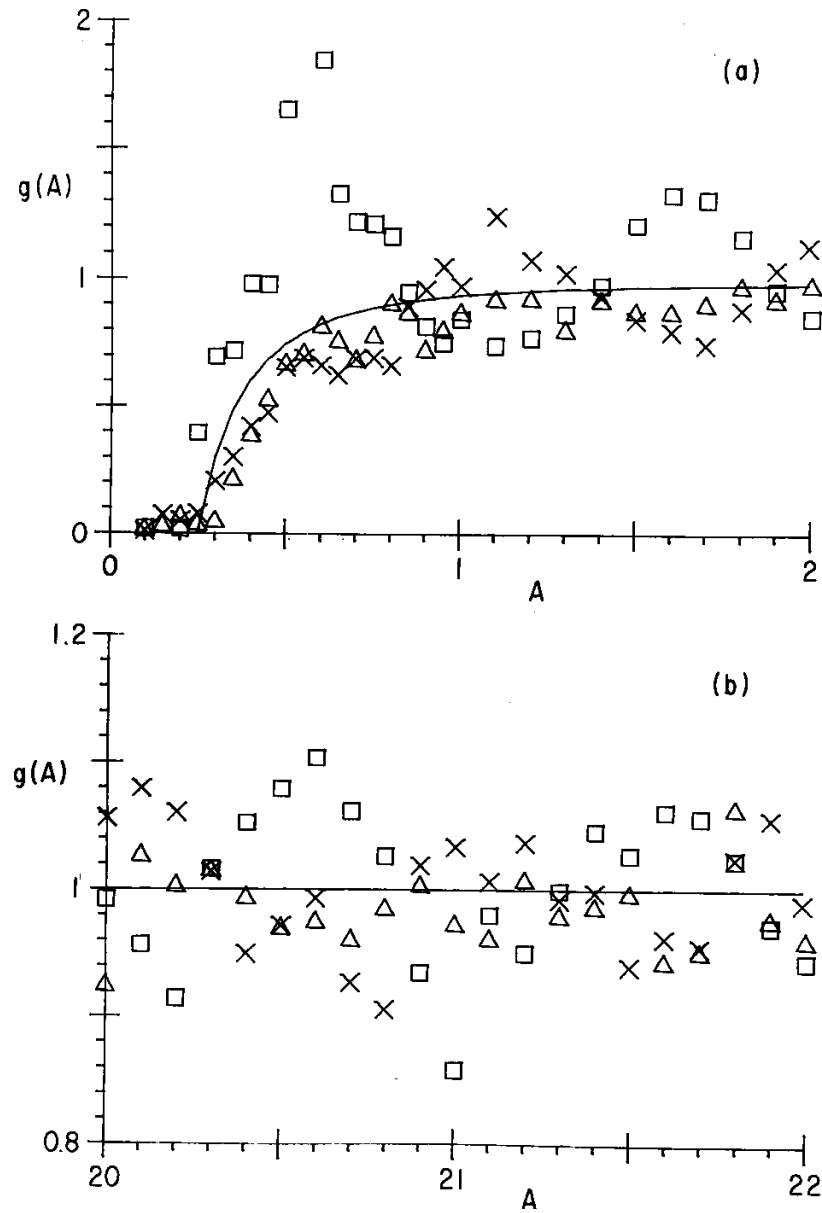
Fig. 9. The function, $g(A)$, against A for $\delta = 0.11$ (crosses), 0.23 (triangles), and 0.47 (squares). (a) and (b) show two different ranges of A. The point for $\delta = 0.47$ and $A = 0.55$ is at $g(A) = 2.8$, and so lies off the scale in (a). The function, g, was evaluated using (55) and (56) with $M = 20$, $L = 2500$, and (a) $K' = 100$, $K = 150$, (b) $K' = 50$, $K = 100$. The solid line gives the approximate form for g, (57).
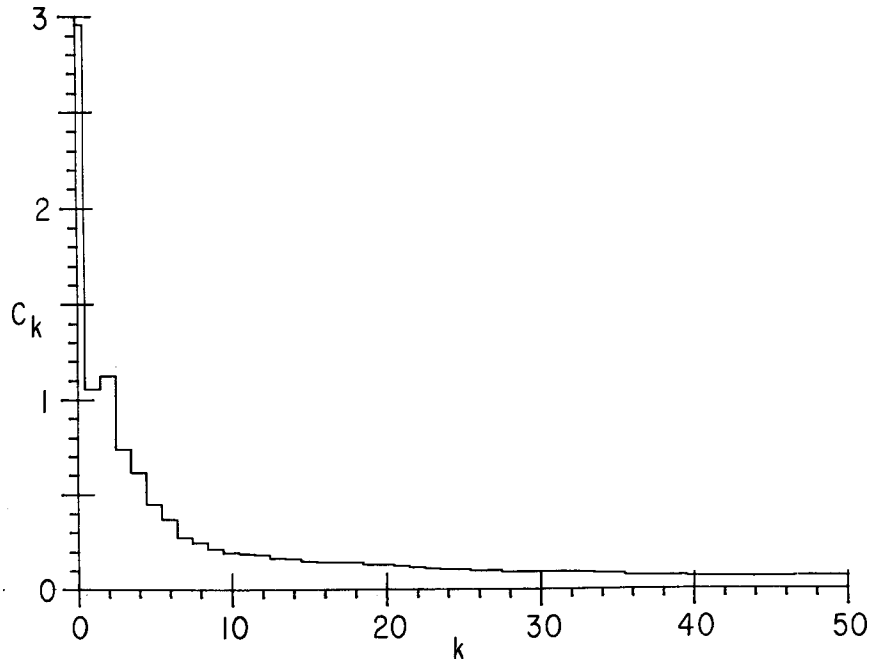
Fig. 10. The correlation function C_k for $\delta = 0.47$, $A = 0.55$, when an accelerator mode is present. Here we took $M = 100$ and $L = 5000$ in (53). The orbits used to compute C_k all lay outside the accelerator mode.
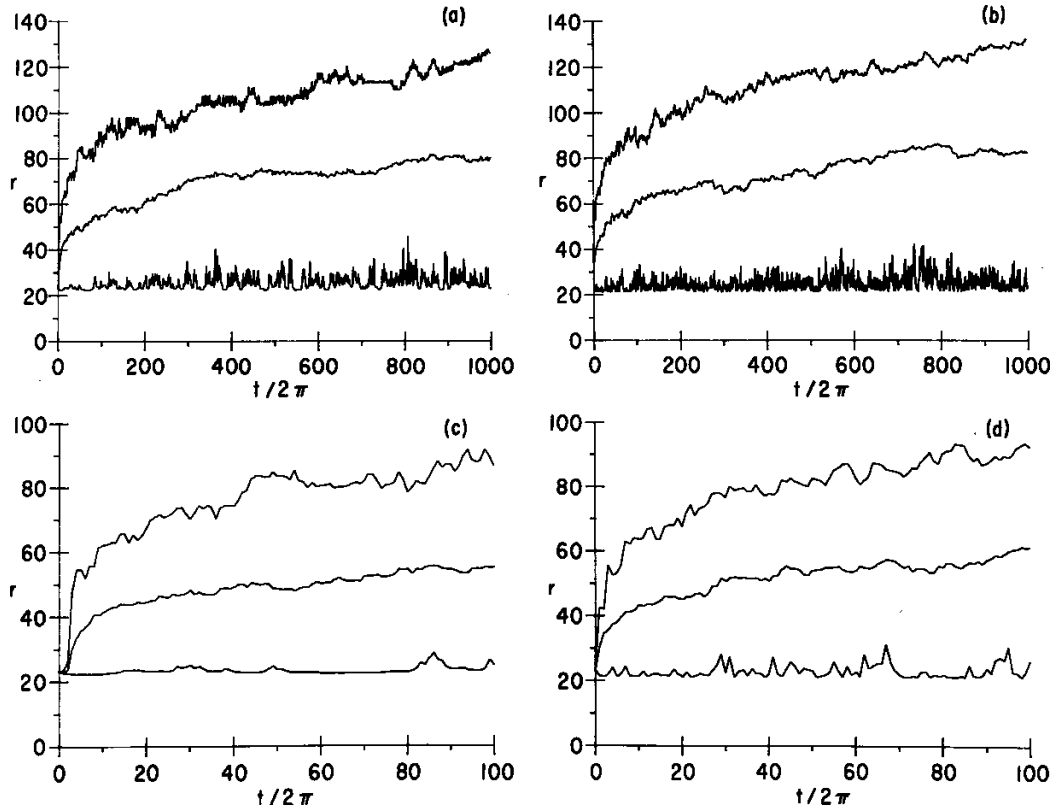
Fig. 11. Maximum, minimum, and rms velocities of ions as given by, (a) and (c), solution of the exact equations of motion, (2) (taken from I), and, (b) and (d), a Monte Carlo solution of (66). In both cases the orbits of $N = 50$ particles were followed with $\alpha = 20$, $\nu = 30.23$, and initial velocity, $r_0 = 23$. In (c) and (d) the time scale is altered to show the short time behavior more clearly.
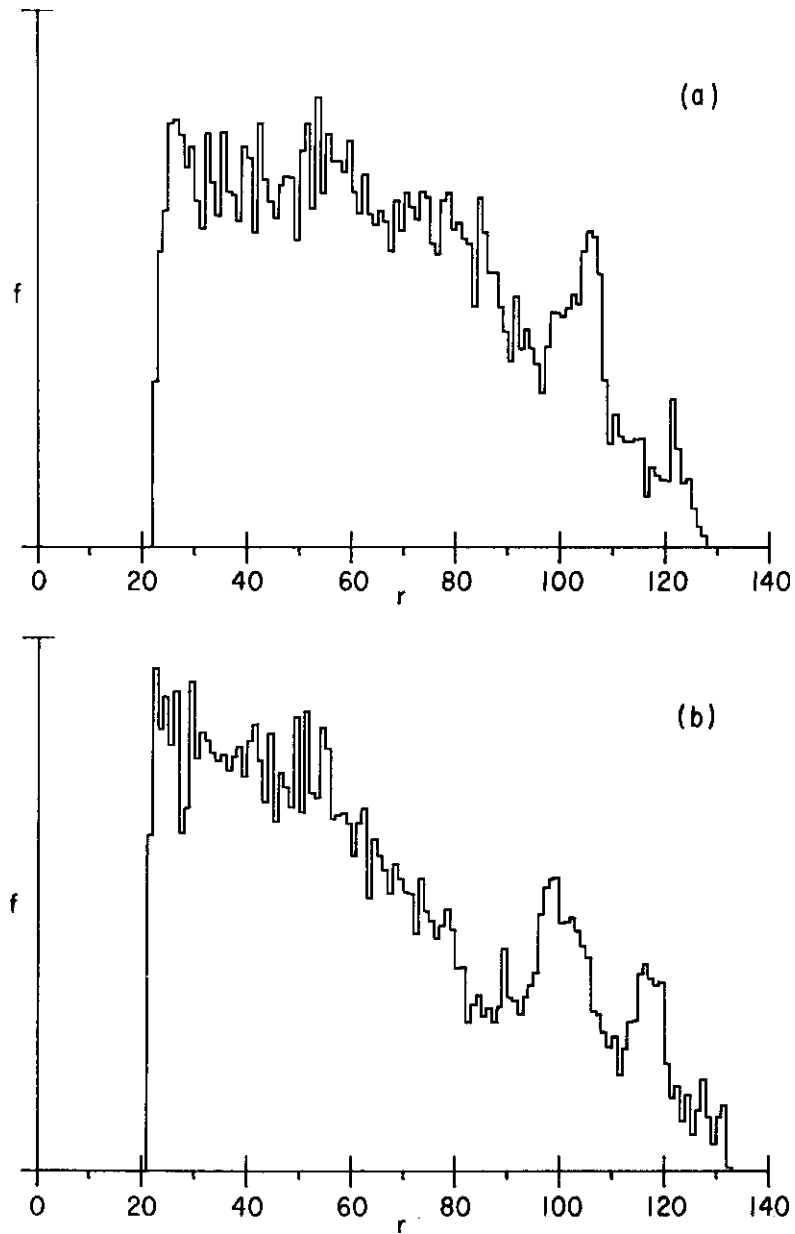
Fig. 12. The perpendicular velocity distribution function for the particles in Fig. 11 averaged over orbits 800–1100. (a) The distribution function obtained from the exact equation, (2) (taken from I). (b) The distribution function obtained from (66). In each case the normalization is such that $\int 2\pi r f \, dr = 1$.
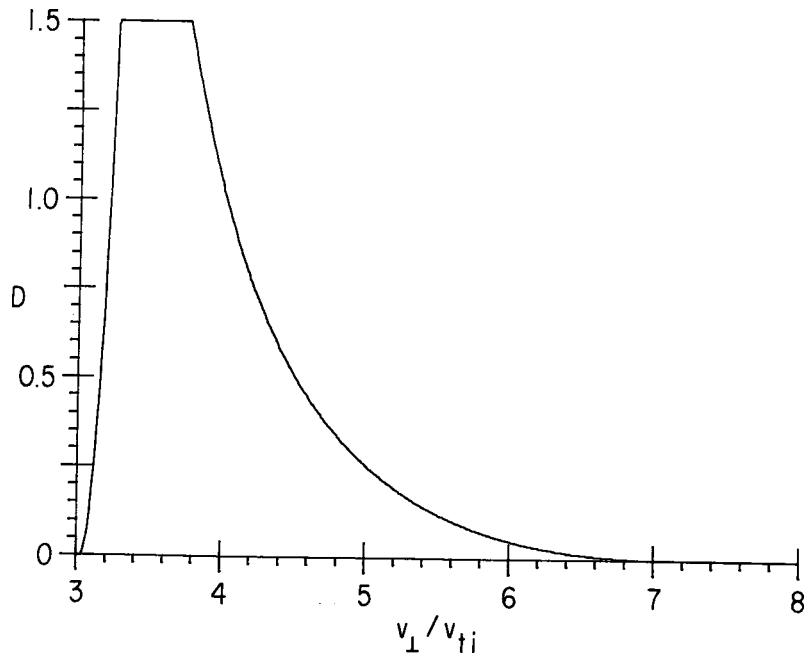
Fig. 13.   The diffusion coefficient D, (69), as a function of $v_\perp$ for the case discussed in Sec. XI.
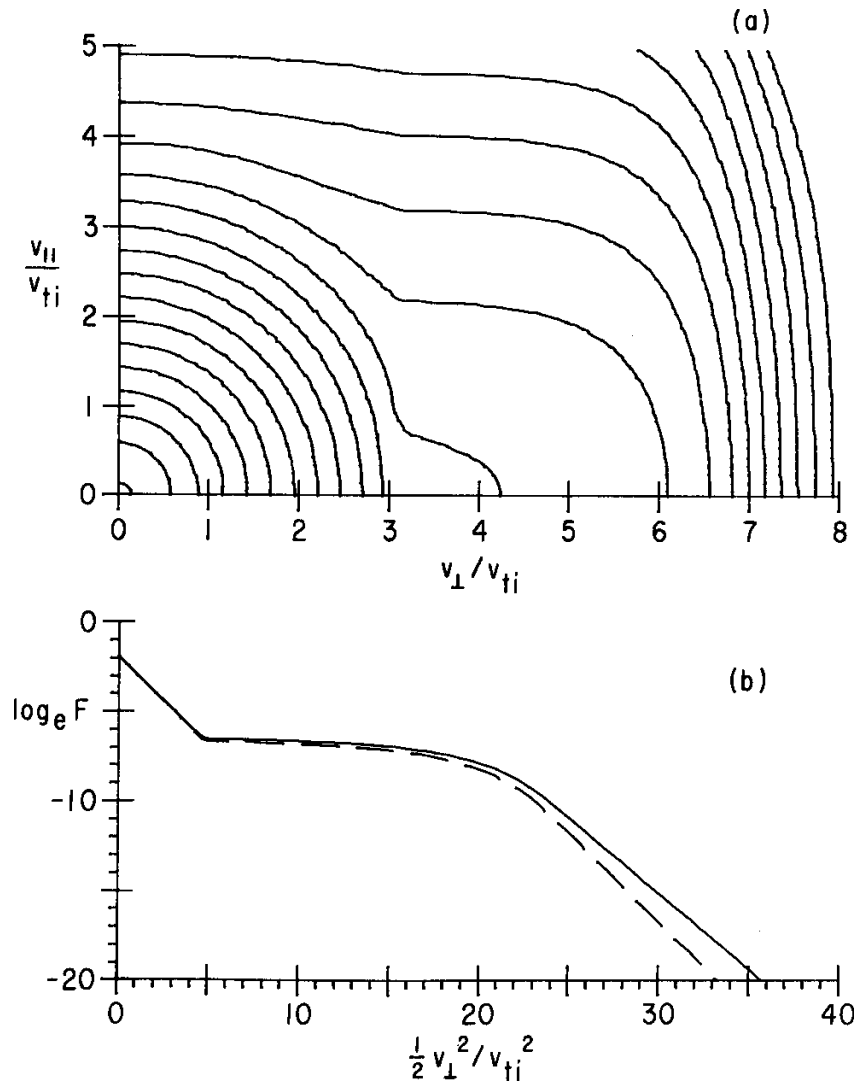
Fig. 14. The steady-state solution for the distribution function. (a) The two-dimensional distribution function, f, as given by the two-dimensional Fokker–Planck equation. (b) The one-dimensional distribution function, $F(v_\perp)$, as given by integrating the two-dimensional result over $v_\parallel$ (solid line) and solving the one-dimensional Fokker–Planck equation (dashed line).
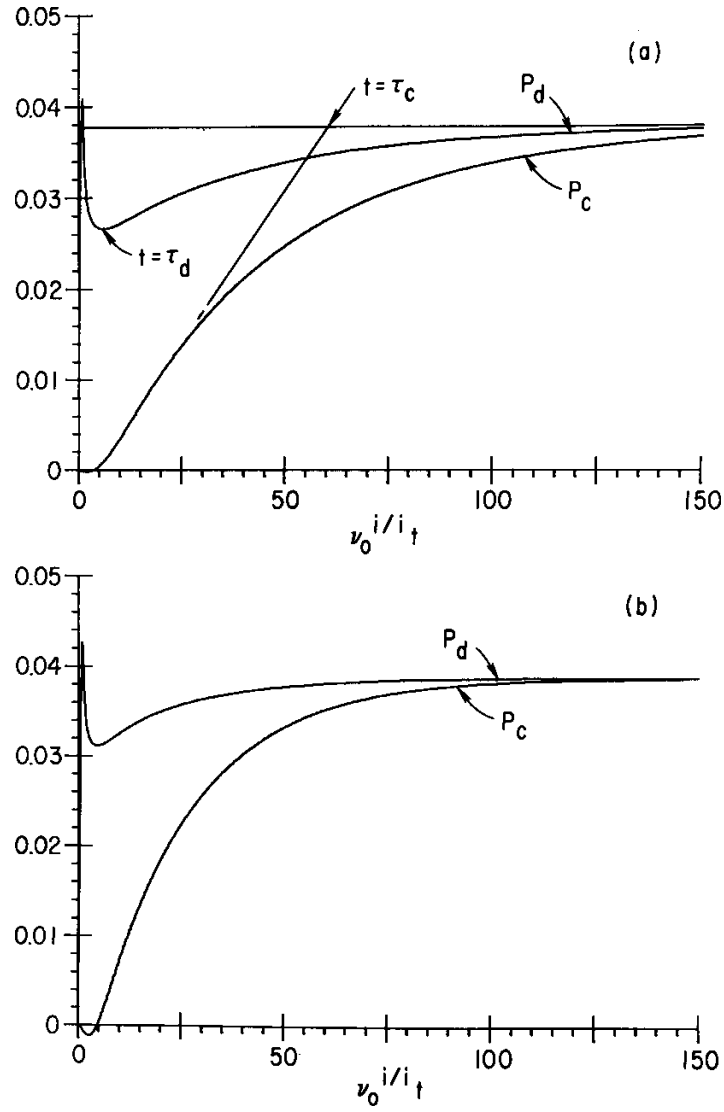
Fig. 15. The power dissipated by the wave, P_d, and the power lost to the background distributions, P_c, as a function of time for the example given in Sec. XI. The results for the two-dimensional and one-dimensional cases are given in (a) and (b) respectively. The units of the vertical axes are $m_i v_{ti}^2 n_0 \nu_0^{i/i}$. The times τ_d and τ_c are shown in (a).
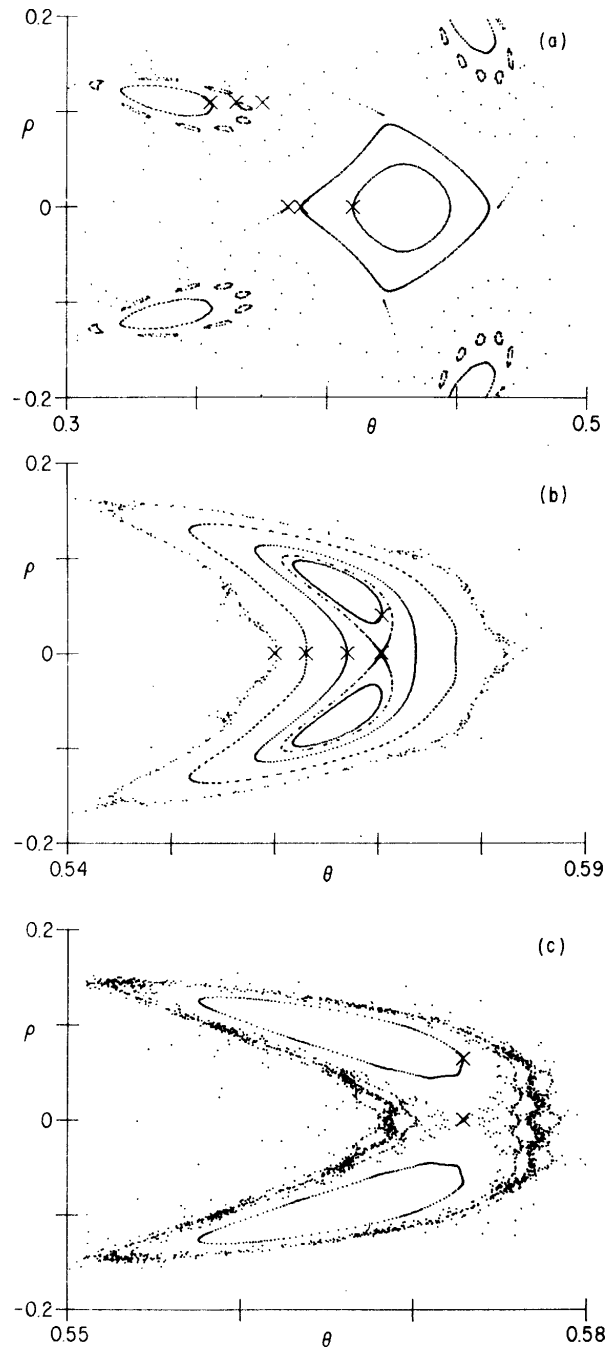
Fig. 16.   Development of the first-order accelerator mode with $m = 1$, $n = 0$, and $\delta = 0.5$. The cases shown are (a) $A = 0.55$, (b) $A = 0.594$, and (c) $A = 0.595$. For this mode $A_\ell = 0.5$ and $A_u = 0.5927$. The crosses show the starting positions of the particles.
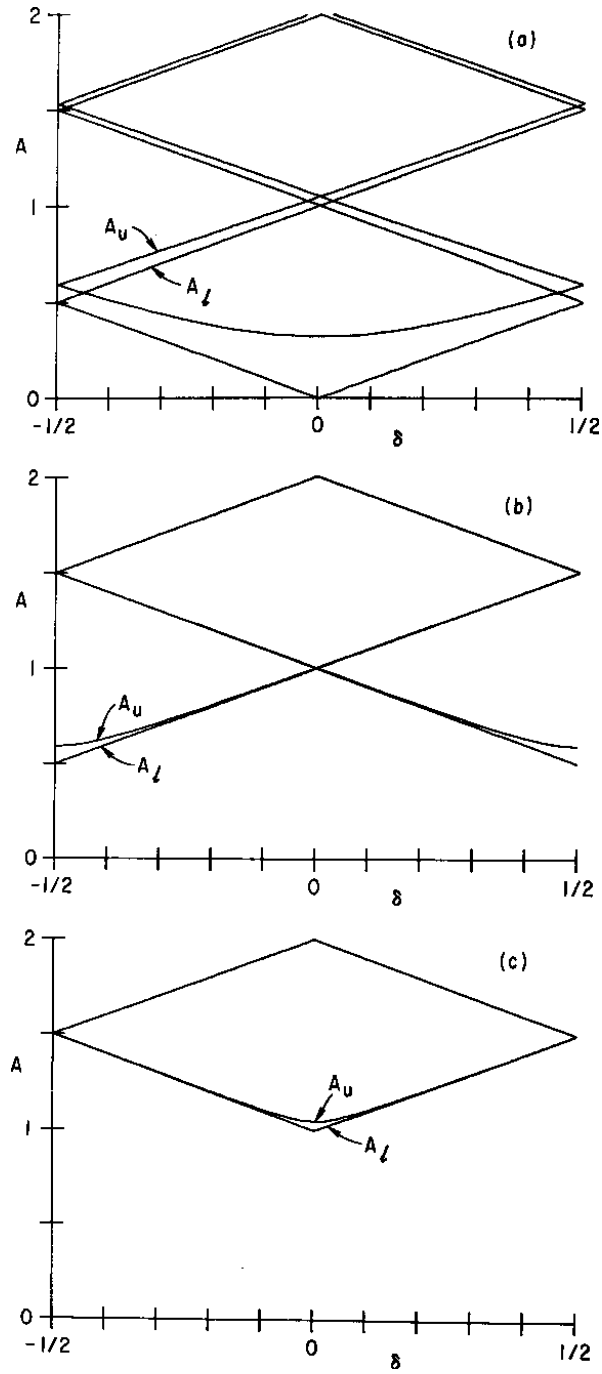
Fig. 17. The range, (A_ℓ, A_u), in which first-order accelerator modes exist with (a) $s = 0$, (b) $s = 1$, and (c) $s = 2$.
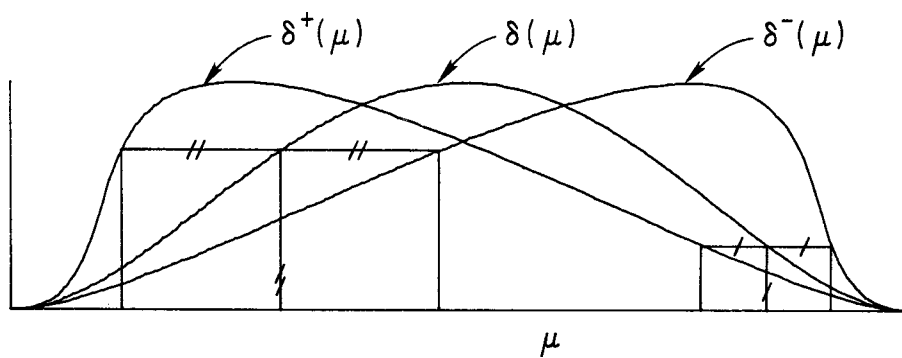
Fig. 18. The graphical construction for $\delta^+(\mu)$ and $\delta^-(\mu)$ from $\delta(\mu)$; see (C8).